Cell Reports

Article

Phase locking of hippocampal CA3 neurons to distal CA1 theta oscillations selectively predicts memory performance

Graphical abstract

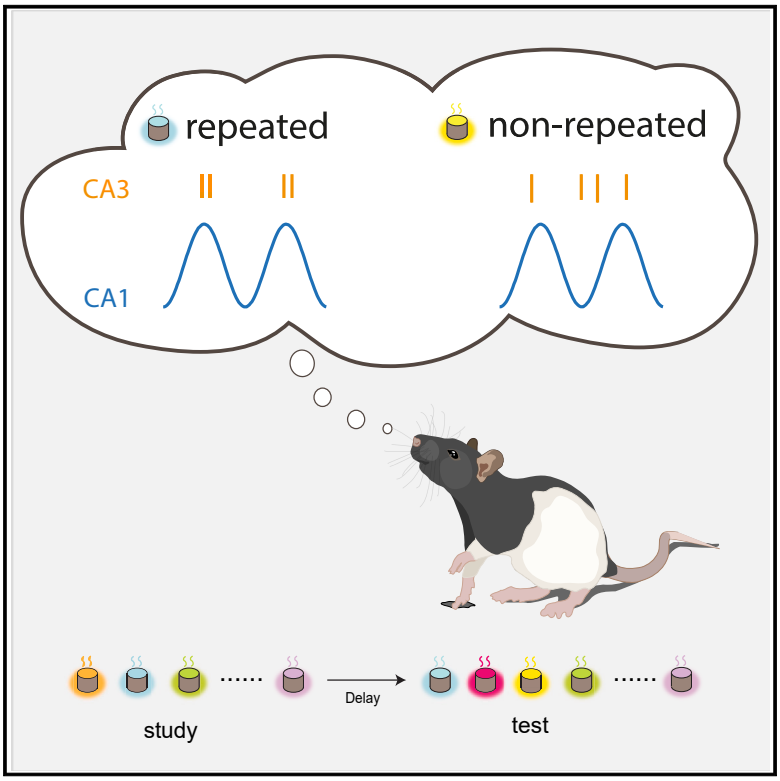

Highlights

- Cross-regional CA3 spike-distal CA1 theta phase locking predicts performance in this task
- CA1 theta power is enhanced during non-spatial memory, especially in distal CA1
- Neurons in distCA1 and proxCA3 are more relevant for SVM analysis of non-spatial memory

Authors

Shih-Pi Ku, Erika Atucha, Nico Alavi, ..., Motoharu Yoshida, Jozsef Csicsvari, Magdalena M. Sauvage

Correspondence

shihpi@gmail.com (S.-P.K.), magdalena.sauvage@gmail.com (M.M.S.)

In brief

Ku et al. showed that synchronization of CA3 neuronal activity with CA1 theta oscillations plays an important role during the recall phase of a high-memory-demand task and revealed the existence of strong CA1 and CA3 proximodistal gradients during this non-spatial task.

Ku et al., 2024, Cell Reports *43*, 114276
June 25, 2024
https://doi.org/10.1016/j.celrep.2024.114276

CellPress

Cell Reports

CellPress
OPEN ACCESS

Article

Phase locking of hippocampal CA3 neurons to distal CA1 theta oscillations selectively predicts memory performance

Shih-Pi Ku,[1,*] Erika Atucha,[1] Nico Alavi,[1] Halla Mulla-Osman,[1] Rukhshona Kayumova,[1] Motoharu Yoshida,[1,2] Jozsef Csicsvari,[3] and Magdalena M. Sauvage[1,4,5,6,*]

[1]Leibniz Institute for Neurobiology, Functional Architecture of Memory Department, Magdeburg, Germany
[2]German Center for Neurodegenerative Diseases (DZNE), Magdeburg, Germany
[3]Institute of Science and Technology (IST), Klosterneuburg, Austria
[4]Otto von Guericke University, Medical Faculty, Functional Neuroplasticity Department, Magdeburg, Germany
[5]Center for Behavioral Brain Sciences (CBBS), Magdeburg, Germany
[6]Lead contact
*Correspondence: shihpi@gmail.com (S.-P.K.), magdalena.sauvage@gmail.com (M.M.S.)
https://doi.org/10.1016/j.celrep.2024.114276

SUMMARY

How the coordination of neuronal spiking and brain rhythms between hippocampal subregions supports memory function remains elusive. We studied the interregional coordination of CA3 neuronal spiking with CA1 theta oscillations by recording electrophysiological signals along the proximodistal axis of the hippocampus in rats that were performing a high-memory-demand recognition memory task adapted from humans. We found that CA3 population spiking occurs preferentially at the peak of distal CA1 theta oscillations when memory was tested but only when previously encountered stimuli were presented. In addition, decoding analyses revealed that only population cell firing of proximal CA3 together with that of distal CA1 can predict performance at test in the present non-spatial task. Overall, our work demonstrates an important role for the synchronization of CA3 neuronal activity with CA1 theta oscillations during memory testing.

INTRODUCTION

Retrieving memories for previously encountered objects, odors, people, or places is crucial for dealing with daily-life situations. In humans and animals, this ability relies heavily on the hippocampus, whose anatomy and functional role are largely conserved across species.[1–7] The hippocampus comprises distinct functional domains, such as the hippocampal subfields CA1 and CA3, which are part of the anatomical pathway that is the most scrutinized for its contribution to memory (the "trisynaptic loop") and features extensive anatomical projections from CA3 to CA1.[8–12] An important focus in memory research has been to elucidate the mechanisms supporting memory. How neuronal spiking activity coordinates local and interregional oscillations has drawn much attention.[13–20] However, whether these functional relationships contribute to memory performance in a decisive manner remains unclear.

Theta oscillations (centered at 8 Hz) are prominent in the hippocampus and have been shown to play an important role in memory function.[21,22] In rodents, theta oscillations facilitate memory processes by coordinating signals within or between areas as seen with the precession of neuronal firing in relation to theta phase as a function of an animal's experience.[23–27] This is also illustrated by the synchronization of spiking activity with theta oscillations between the hippocampus and the prefrontal or the entorhinal cortex.[28–34] In humans, the amplitude of theta oscillations varies in a task-dependent manner, and memory performance improves when stimuli are presented at a theta frequency.[35–38]

A tremendous amount of knowledge has been accumulated on local couplings within the hippocampal subfields CA1 or CA3 (i.e., spike-to-theta phase locking within CA1 or CA3) in rodents in studies investigating spatial navigation using tasks such as running on a linear track.[24,27,39–42] In contrast, the relationship between theta oscillations and neural spiking activity *between* hippocampal subregions and its ties to memory performance are not yet well understood. Hence, whether the coordination of CA3 neuronal spiking activity with CA1 theta oscillations (i.e., CA3 spike to CA1 theta phase coupling) bears an important role in recognition memory remains elusive, especially in tasks that are devoid of salient spatial information with high memory load that are often used in humans.[43–46]

During the past decade, immediate-early gene imaging and electrophysiological studies have provided robust evidence for a functional segregation of spatial and object/odor information processing along the proximodistal axis of CA1 and CA3.[47–53] These findings suggest that distinct subnetworks exist within the hippocampus that would preferentially process either spatial or

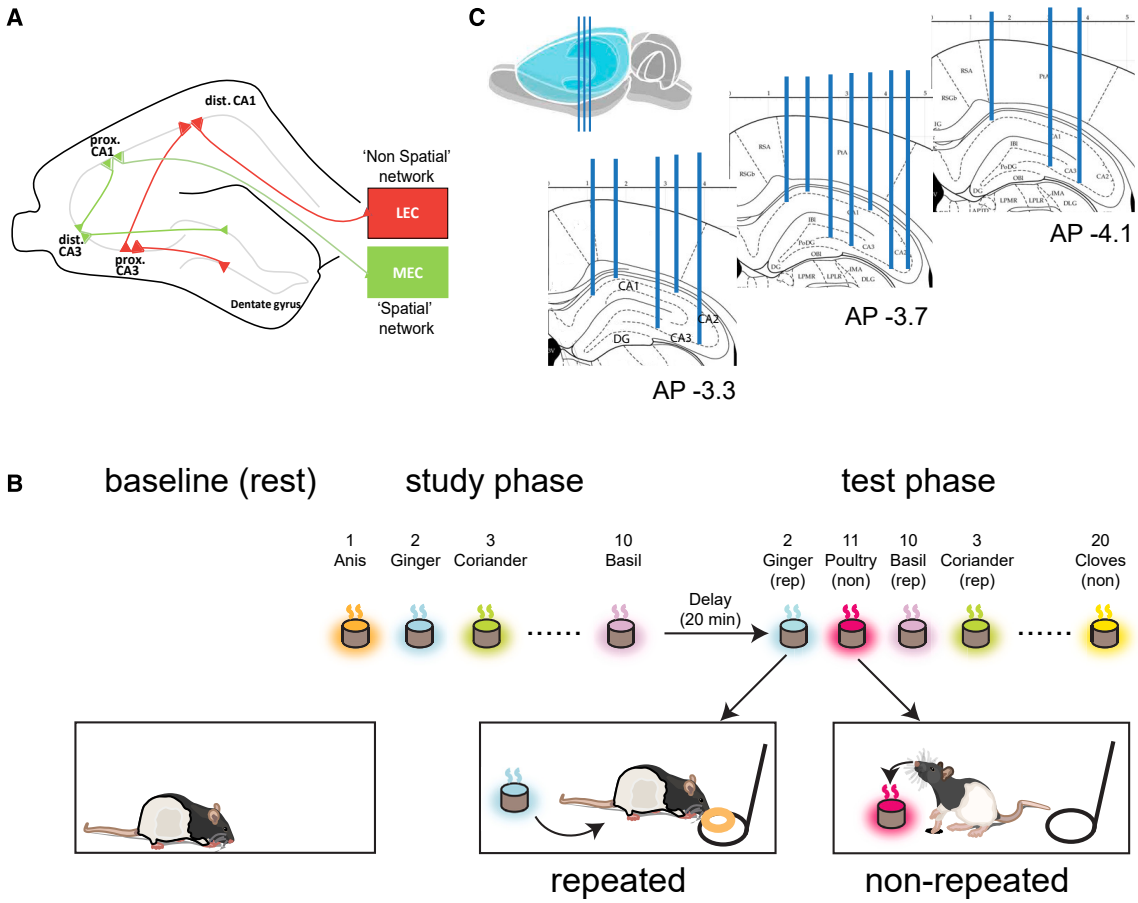

Figure 1. Schema of the "spatial" and "non-spatial" subnetworks of the hippocampal region, odor recognition memory paradigm, and hippocampal recording sites

(A) The "segregated paths" model describing subnetworks preferentially processing spatial and non-spatial information: the "spatial" and the "non-spatial" subnetworks (in green and red, respectively).[47,51] The non-spatial subnetwork includes the lateral entorhinal cortex (LEC), proximal CA3 (proxCA3), distal CA1 (distCA1), and the exposed blade of the dentate gyrus (exp. DG). The spatial subnetwork includes the medial entorhinal cortex (MEC), distal CA3 (distCA3), proximal CA1 (proxCA1), and the enclosed blade of the DG (encl. DG).

(B) Delayed non-matching to odor memory task: each day, the session started with rats resting in their home cage placed in the recording booth for 20 min (baseline). Thereafter, rats sampled 10 different odors, one by one, during the study phase (the study list changed each day). After a 20-min delay, the memory for these odors ("repeated" odors) was tested by presenting to the rats the same odors intermixed with 10 other odors that had not been experienced during the study phase (i.e., "non-repeated" odors), one by one and in a pseudorandom manner. Both repeated and non-repeated odors were part of a pool of 40 familiar odors that had been used in a pseudorandom manner over the 2 months of training. According to a non-matching to sample rule, rats report a repeated odor by refraining from digging and turning away from the stimulus cup (i.e., a correct response) and a non-repeated odor by digging into the stimulus cup (i.e., a correct response). Memory performance (percent correct) was calculated on the basis of these responses.

(C) Recording sites were located at the tips of the blue parallel lines and distributed along the entire proximodistal axis of CA1 and CA3 at approximately AP −3 to −4 mm from bregma.

non-spatial information: the "spatial" subnetwork including distal CA3 (distCA3) and proximal CA1 (proxCA1) and the "non-spatial" subnetwork including proxCA3 and distCA1 (Figure 1A[47,51]). However, *in vivo* evidence for such subnetworks as well as evidence of a functional interaction within these subnetworks is missing.

Here, we examined the relationship between neuronal activity and theta oscillations *in vivo* both within and between CA3 and CA1 and its ties to memory performance. In an attempt at bridging further human and animal recognition memory, we leveraged a high-demand-memory task adapted from humans to rats,[51,54,55] simultaneously recorded the electrophysiological activity along the proximodistal axis of CA1 and CA3, and analyzed neuronal activities at population and single-cell levels. In humans, recognition memory tasks typically consist of presenting a list of stimuli, for example words appearing one at a time in the center of a screen consecutively, to which memory for these stimuli is evaluated. This evaluation is done by presenting sequentially the same stimuli ("repeated") intermixed with stimuli that were not part of the study list ("non-repeated") and calculating the percentage of correct responses.[43–46] In a similar manner, here, we examined the memory for a series of stimuli experienced during a study phase in rats by presenting at test

the same stimuli (repeated stimuli) intermixed with stimuli that rats had not experienced during the study phase (non-repeated stimuli) (Figure 1B). Given that olfaction is the primary sense of rodents and that rats have an exceptional memory capacity for odors, odors from a pool of forty common household scents were used as stimuli.

We found that the spiking activity of CA3 neurons was selectively phase locked close to the peak of distal CA1 theta oscillations during the retrieval of the memory of a previously encountered stimulus (repeated stimulus) but not when the stimulus was not experienced during the study phase (non-repeated). We also show that the population phase information of CA3 spikes predicted memory performance trial by trial only when theta was referenced to the distal part of CA1. Our results suggest that the coordination of CA3 activity with CA1 theta rhythm may constitute one of the fundamental mechanisms supporting memory retrieval and indicate a preferential involvement of proximal CA3 and distal CA1 in processing non-spatial memory.

RESULTS

Local field potential (LFP) and single-unit activity in CA1 and CA3 were simultaneously recorded in the same animals (5 rats; 633 neurons: 394 in CA1 and 239 in CA3; Table S1A) from up to 16 sites using tetrode arrays covering the transverse (proximodistal) axis of CA1 and CA3 (Figure 1C; see STAR Methods for localization of the tetrodes and clustering criteria). Population activity, single-cell firing and characteristics of theta oscillations (amplitudes), as well as cross- (CA3-CA1) or within-area (CA1-CA1 or CA3-CA3) spike-theta phase-locking properties and their relationships to memory performance, were studied in the same behavioral arena at baseline (i.e., prior to the study phase) as well as during the study and the test phase of the task (Figure 1B; see STAR Methods; Figure S1: analysis epochs).

A proximodistal gradient in population activity discriminating repeated from non-repeated odors trial by trial

Discrimination between stimuli or spatial contexts has been recently reported to be coded at the population level rather than by individual cell firing.[20,56,57] Hence, we first investigated whether population activities (i.e., the combined mean firing rate of individual neurons) could reflect discrimination between repeated and non-repeated odors during the test phase of the task trial by trial. The period analyzed started upon stimulus presentation (when the front edge of the stimulus platform crossed the wall of the cage) and ended 2 s later, before behavioral response (turning or digging; the time window of 2 s was defined based on prior experiments showing that behavioral response in this task occurs shortly after 2 s; see Figure S1 for exact time windows). Rats were alertly waiting during this 2-s period. We used a support vector machine (SVM) algorithm to analyze the population activities of all recorded neurons in each animal at test (n = 127 neurons on average per animal; Table S1A).[58,59] First, we tested whether the SVM classification performance of all neurons would match the animal's memory performance, which would indicate an important contribution of hippocampal population cell firing to memory retrieval. In agreement with literature, we found this was the case (Figure 2A, blue and white bars; averaged SVM performance of all neurons: 75% correct; averaged animal memory performance: 80% correct, n = 5; SVM vs. memory performance: $t_4 = 1.414$, $p = 0.230$, paired t test; Table S1A; SVM > chance level: $t_4 = 7.905$, $p = 0.001$, one-tailed t test). Second, we observed that only population cell firing of the areas belonging to the hippocampal subnetwork preferentially processing non-spatial information (proxCA3+distCA1) could account for the classification performance of all recorded neurons, indicating a prominent role of cell firing at the population level in proxCA3 and distCA1 for odor memory retrieval (Figures 2A and 2B; SVM performance [proxCA3+distalCA1]: 77%; compared to all neurons: $t_4 = 0.302$, $p = 0.778$, paired t test; SVM > chance level: $t_4 = 5.511$, $p = 0.005$; one-tailed t test, proxCA3+distCA1 neurons represent ~69% of the recorded neurons; SVM performance [distCA3+proxCA1]: ~54%; compared to all neurons: $t_3 = -2.852$, $p = 0.033$; paired t test; SVM > chance level: $t_3 = 0.522$, $p = 0.638$, one-tailed t test, all comparisons false discovery rate [FDR] corrected; see Table S1A). Moreover, the SVM classifier for the areas belonging to the counterpart subnetwork (distCA3+proxCA1) performed significantly lower than the classifier for proxCA3+distCA1 (paired t test, $t_3 = -2.435$, $p = 0.047$), supporting the hypothesis that proxCA3 and distCA1 might be more engaged than distCA3 and proxCA1 for retrieving non-spatial (odor) memory.

Furthermore, we tested whether population firing activities of all neurons could predict behavioral responses per se (i.e., digging or turning independently of whether animals responded correctly or not). We found that population firing activities of all neurons did not account for digging or turning per se (Table S1A; averaged SVM performance for behavioral responses: 59%; SVM > chance level: $t_4 = 0.91$, $p = 0.181$).

We also found that all recorded neurons did not contribute to the same extent to the population classification performance by using an iterative feature selection procedure, deleting neurons one at a time to assess if the deletion of a specific neuron affects the population performance (Figure S3). For each iteration, one neuron was removed from the whole population ($n = N$) in a given animal, and the rest of the population ($n = N - 1$) underwent SVM classification analysis. If the performance of the remaining population ($n = N - 1$) was lower than the performance of the whole population ($n = N$), the removed neuron was termed "effective." Otherwise, it was termed "non-effective" (see Figure S3 and STAR Methods for the iterative procedure). On average, 7% of the neurons recorded in each animal were deemed effective (i.e., on average 9 effective vs. 117 non-effective neurons per animal, 47 vs. 586 in total across animals; Table S1A). The classification performance across animals for these effective neurons was higher than that of the rest of the neurons (effective vs. non-effective neurons: $t_4 = 2.971$, $p = 0.041$, paired t test; light blue vs. gray bar; Figure 2C), as expected given the selection process. What the selection process could not account for, however, is that the performance of this 7% of neurons (n = 9 on average) was comparable to that of all recorded neurons (n = 127 on average; mean SVM performance effective neurons = 85% correct; effective vs. all: $t_4 = 1.907$, $p = 0.129$, light vs. dark blue bar; of note, this was not the case for non-effective neurons vs. all: $t_4 = -3.361$, $p = 0.028$, paired t tests, Figure 2C, gray vs.

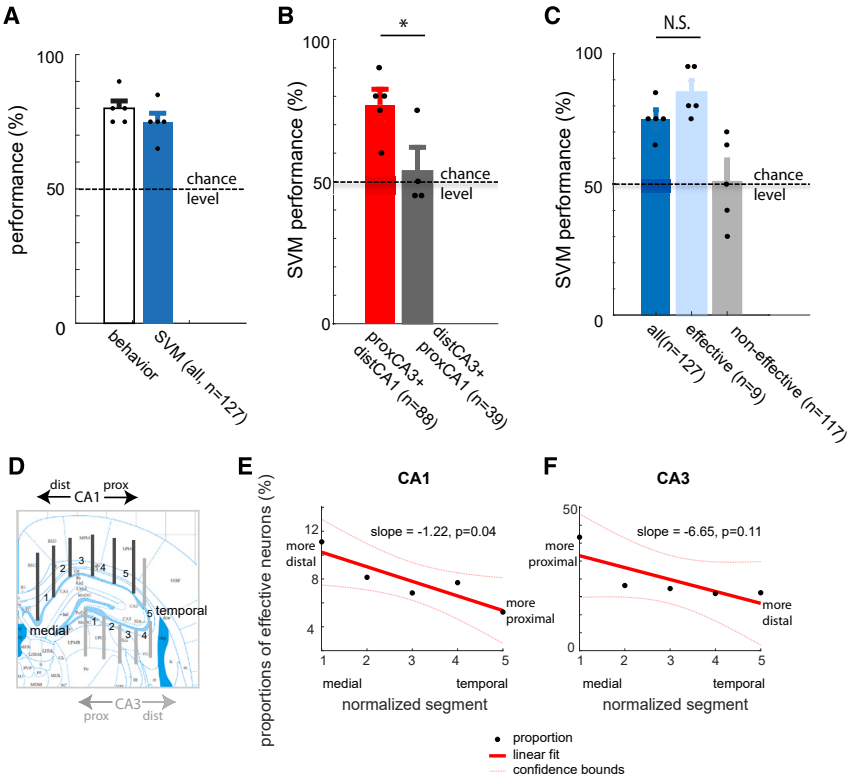

Figure 2. Memory and SVM performance: Topographical distribution of "effective" neurons along the proximodistal axis of CA1 and CA3

(A) Memory performance on the recording day and population classification performances of all neurons discriminating between "repeated" and "non-repeated" stimuli (across the 5 recorded rats) obtained using a support vector machine (SVM) algorithm. Rats were trained until they reached a plateau performance of at least 75% correct choices over 3 consecutive days; subsequently, single-cell firing and LFP were recorded during an additional session with above-threshold (75% correct) behavioral performance. The population classification performance of all neurons could account for the behavioral memory performance. Dots indicate the performance for individual rats ($N = 5$).

(B) SVM population classification performances across the 5 recorded rats based on neurons belonging to the "non-spatial" subnetwork (proximal CA3+distal CA1) or to the "spatial" subnetwork (distal CA3+proximal CA1). Only the population classification performance of the neurons belonging to the non-spatial subnetwork (proxCA3+distCA1) was comparable to the SVM performance of all recorded neurons. Moreover, SVM performance of proxCA3+distCA1 was higher than that of neurons belonging to the spatial subnetwork (distCA3+proxCA1). Averaged cell counts per animal are in brackets and rounded up or down for clarity (see Table S1A).

(C) The SVM performance of "effective" neurons (on average $n = 9$ neurons per rat) but not that of the "non-effective" neuron population could also account for the SVM performance of all recorded neurons and memory performance.

(D) Anatomical location of the five proximodistal segments of CA1 and CA3 in which neural activities were recorded. Segment 1 is more medial and segment 5 more temporal (see STAR Methods for segment normalization procedure). In CA1, segment 1 is the most distal and segment 5 the most proximal; in CA3, segment 1 is the most proximal and segment 5 the most distal.

(E and F) Distribution of the proportions of effective neurons along the proximodistal axis of either CA1 (E) or CA3 (F). In CA1, the slope of the linear regression was significantly smaller than zero ($p = 0.04$), indicating a distal to proximal gradient of the distribution of effective neurons in CA1 (higher proportion in distal CA1). In CA3, although the slope failed to reach significance, comparing the two most proximal (1 and 2) to the two most distal (4 and 5) segments of CA3 indicated a larger proportion of effective neurons in the most proximal part. Altogether, these data indicated a prominent role of population cell firing in proximal CA3 and distal CA1 (the non-spatial subnetwork) during the test phase of the odor memory task when compared to that of distal CA3 and proximal CA1 parts of the spatial subnetwork. Dots, proportions of effective neurons in each segment; red line, linear fit; red dotted lines, 95% confidence bounds. Error bars: SEM. *$p < 0.050$.

dark blue bar), and that SVM performance of the remaining non-effective neurons ($n = 117$ on average) would not differ from chance level (mean SVM performance of non-effective neurons = 51% correct; $t_4 = 0.134$, $p = 0.900$), while the classifier performance of effective neurons did (comparison to chance level: $t_4 = 8.367$, $p = 0.001$, one-sample t test, Figure 2C). Hence, these results indicate that population firing activities of about 7% of the recorded neurons (47/633, effective neurons/all neurons across animals) can account for the SVM classification performance of all recorded neurons (Figure 2C; Table S1A).

Moreover, the topographical distribution of the effective neurons was not homogeneous along the proximodistal axis of CA1 and CA3 (Table S2). In CA1, the distribution of effective neurons linearly decreased from distal to proximal (Figures 2D and 2E; $p = 0.040$, slope different from zero; Table S2). In CA3, although the distribution did not linearly decrease from proximal to distal when all segments were taken into consideration (Figure 2F; $p = 0.110$), a direct comparison between the two most medial and the two most temporal segments revealed a higher proportion of effective neurons in the proximal than the distal part of CA3 (segments 1–2 vs. segments 4–5: $z = 3.230$, $p = 0.001$, two-proportion z test), bringing further support to the hypothesis of a preferential tuning of proxCA3 and distCA1 (belonging to the non-spatial subnetwork) to the processing of odor information during memory retrieval.

Finally, we examined whether there was a general increase or decrease in firing rates for the retrieval of repeated odors when compared to non-repeated odors in individual CA1 and CA3 neurons. Mean individual firing rates differed between repeated and non-repeated odors in only 41 out of 633 neurons (i.e., 6.5% of all neurons, 8 neurons per animal on average, Table S3; paired t test, threshold at $p < 0.050$, example cell firing patterns in Figure S4; 5 out of the 41 are effective neurons) and did not generally increase or decrease for either stimulus type (4.8 neurons per animal increased and 3.4 decreased, increasing vs. decreasing proportion: $p = 0.270$, two-proportion z test; see Table S3 for individual animals). Combining the firing rates of the neurons with differential firing rates could predict memory performance (SVM

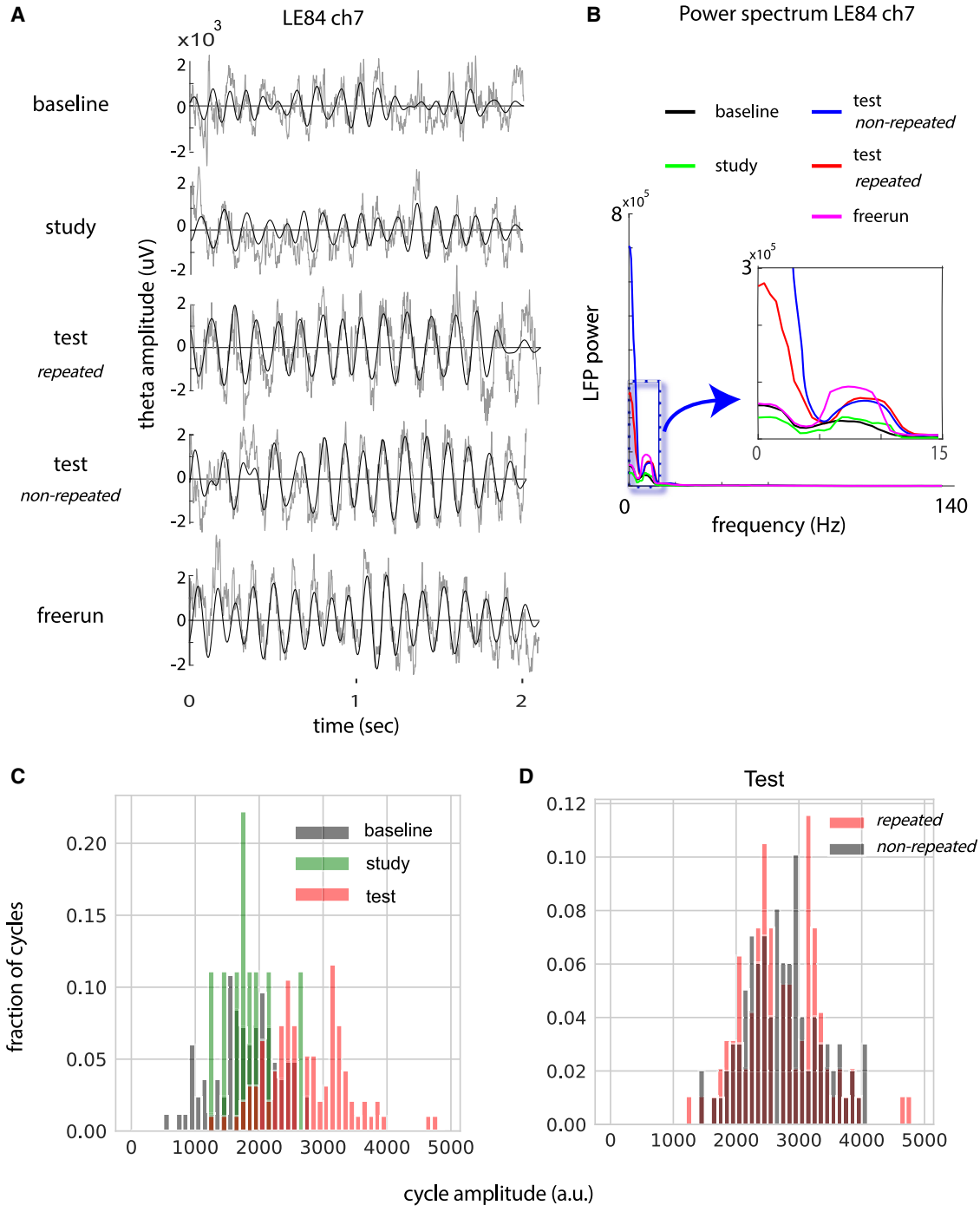

Figure 3. Theta power was high during non-spatial (odor) memory, especially during the test phase

(A) Examples of individual unfiltered local field potential overlaid with filtered theta oscillations (6–12 Hz) of one representative recording session during baseline, study, test, and free run, indicating that theta oscillations are strong during the different phases of the present task, which is devoid of salient spatial components (averaged animal's speed at baseline: 1.63 cm/s; speeds at test and free-run traces were matched: ~5.5 cm/s; animal's speed at study: 8.48 cm/s). Note that even when the animal's speed was higher (study phase), theta amplitudes were lower.

(B) Power spectrum analysis of one example session indicating a higher theta power at retrieval (for both "repeated" [red] and "non-repeated" [blue] trials) and free run (magenta) compared to baseline (black) and study (green).

(legend continued on next page)

performance: 61%, $t_4 = 11$, $p < 0.001$, one-tailed t test to chance level; Table S1B) but to a lower extent than combining the firing rates of effective neurons that are comparable in number ($n = 9$ per animal in average, 47 in total across animals; comparison to SVM performance of effective neurons (i.e., to 85% correct; $t_4 = 5.237$, $p = 0.006$, paired t test; Figure S2). Furthermore, we assessed whether the firing rate, this time, of all CA1 and CA3 neurons (i.e., differentially firing or not) was overall enhanced or suppressed during repeated trials in comparison to non-repeated trials. This was not the case, as CA1 neuronal firing rates were higher for the retrieval of repeated odors than non-repeated odors in only two out of five rats (no differences in CA3 for these rats; no differences in the three remaining rats in either CA1 or in CA3; Figure S5). Taken together with our earlier finding that the proxCA3+ distCA1 population activity can discriminate repeated from non-repeated odors, this indicates that differences in population activity between stimulus types might be a better predictor of memory performance than a general enhancement or suppression of single-cell firing rates.

Altogether, these results show that population activity in distCA1 and proxCA3 alone can account for the population classification performance of all recorded neurons, suggesting that the non-spatial hippocampal subnetwork may play a preponderant role in memory retrieval in this task. Moreover, this finding raises the possibility of a preferential coordination of proxCA3 and distCA1 electrophysiological signals during odor memory retrieval. To further test this hypothesis, we investigated CA3 spikes to CA1 theta phase locking along the proximodistal axis of CA1 and CA3.

Preferential CA3 spike-distal CA1 theta coordination during odor memory test

Theta oscillations in rodent CA1 have been shown to play a crucial role in spatial navigation tasks, while, in comparison, much less is known about their role in non-spatial memory, especially in tasks with high memory demands. Hence, we first studied CA1 theta oscillation characteristics (cycle-by-cycle amplitudes, i.e., power) in the odor task used in the present study. This was done along the proximodistal axis of the hippocampus in the animals previously described. Second, we investigated the relationship between neuronal spiking and theta oscillations between and within CA3 and CA1 and how this relationship could account for memory performance.

CA1 theta oscillation's amplitudes are high during odor memory, especially during the test phase of the task

Theta oscillations in distal CA1 were strong during all phases of the task: i.e., at baseline (resting period before study), study, and test (see Figures 3A and 3B for individual examples of theta oscillations and power spectra and Figure S6 for examples of longer raw traces). At the group level, the frequency of theta oscillations was similar throughout the phases of the task ($F_{2,12} = 0.07$, $p = 0.930$, one-way ANOVA, Table S4). In addition, using a cycle-by-cycle analysis optimized for trials with short durations, as is the case in our task (~2 s[60]), we showed that averaged theta cycle amplitudes (i.e., theta power) were significantly larger in CA1 at retrieval than in study or baseline phases in all animals ($\chi^2_2 = 7.6$, $p = 0.022$, Friedman's test [nonnormal distribution of theta amplitudes]; comparisons within individual animals: all p values < 0.001, Mann-Whitney U tests; see an example of theta cycle amplitudes in Figure 3C; theta amplitudes were also larger in study phase than in baseline: all p values < 0.050; all comparisons FDR corrected; Table S5). In contrast, theta power was comparable for the presentation of repeated and non-repeated odors at test in 4 out of 5 animals ($p > 0.105$ Mann-Whitney U test, Figure 3D; see Table S5 for individual data), and no general pattern could be observed between "pre-trial" and "in-trial" periods of the task (i.e., 2 s before vs. after stimulus delivery at test; theta power was lower before stimulus presentation in 2 rats, higher in 1 rat, and comparable before and after stimulus presentation in the remaining 2 animals; Table S5; see Figure S1 for the description of pre- and in-trial periods and STAR Methods for details) suggesting that theta power was rather homogeneous throughout the retrieval phase of the task.

Because running speed was reported to affect theta power,[21,61–65] we further studied the relationship between the speed of animals in our task and the amplitude of theta oscillations. The average speed significantly differed across task phases ($F_{2,12} = 30.12$, $p < 0.001$, one-way ANOVA, Table S6). The speed at study and test was low, and post hoc analyses revealed that they were comparable across the five animals (median ± std = 4.34 ± 0.03 and 4.69 ± 0.26 cm/s, respectively; $t_8 = 1.412$, $p = 0.260$, two-sample t test) and, as expected, higher than at baseline (1.35 ± 1.38 cm/s; baseline vs. study or test: $p < 0.001$, two-sample t tests: FDR corrected; see Figure S7; Table S6 for individual data). Moreover, a mixed-effect linear model analysis, using task phase, running speed, and their interaction as fixed effects and individual animals as random effect, revealed that theta power was significantly affected by the task phase ($p < 0.001$) but not the running speed ($p = 0.480$; for more details, see STAR Methods, analyses section). This indicates that the phase of the task is more likely than the running speed to contribute to the enhancement of the observed theta amplitudes.

Altogether, these results indicate that theta power is high during the present odor memory task, as has also been previously described during spatial tasks. Moreover, our data show that theta power in distal CA1 is especially high during memory retrieval, that this enhancement lasts throughout the entire test phase of the task, and that the increase in the amplitude of theta oscillations is unlikely to stem solely from changes in movement speed.

Theta power is higher in distal CA1 than proximal CA1 in trained, but not naive, rats

We also found that the amplitude of theta oscillations in the five trained rats was higher in distal than proximal CA1 (all p

(C) Example distributions of the amplitude of each theta cycle during baseline, study, and retrieval in one representative animal. Cycle-by-cycle analyses optimized for short duration trials[60] revealed that averaged theta cycle amplitudes (i.e., theta power) were enhanced during the test phase of the task compared to baseline or study.

(D) In contrast, theta power was comparable at test of either type of stimulus as revealed by the overlapping distribution of theta cycles' amplitudes for repeated and non-repeated odors. A.u., arbitrary unit.

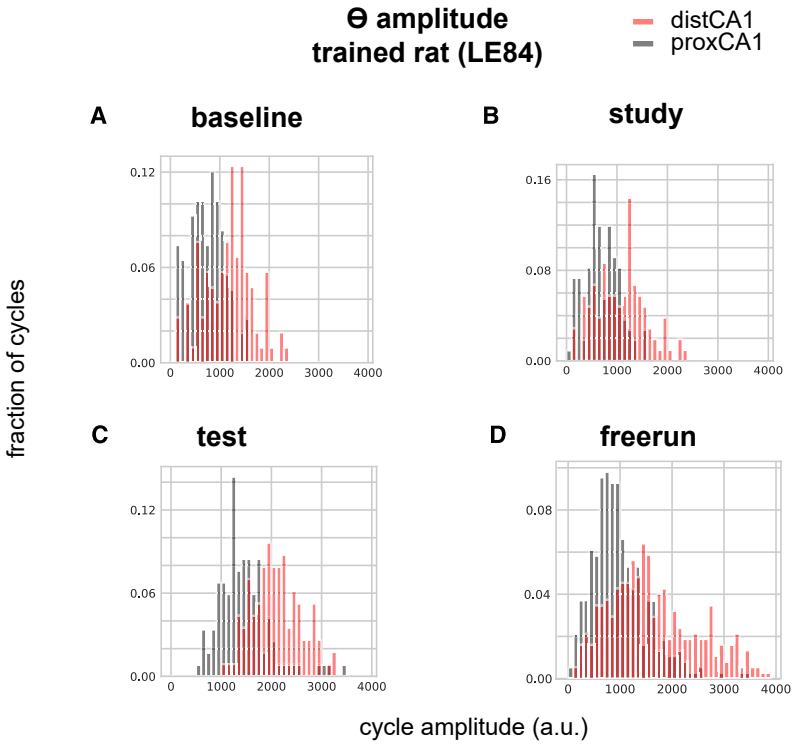

Figure 4. The distributions of the amplitude of theta cycles in distal and proximal CA1 in representative trained or naive rats

(A–D) The amplitudes of theta cycles (power) were enhanced in distal CA1 when compared to proximal CA1 in all phases of the task as well as during free run when the animal has been trained (over 2 months) on the odor memory task.

(E) In contrast, theta power was comparable in distal and proximal CA1 in naive animals during baseline (resting period).

(F) Differences in the amplitude of theta cycle between distal and proximal CA1 were obtained using the Kolmogorov-Smirnov test to generate the D value (Maximum$|Fo_x - Fr_x|$, F_x = observed cumulative frequency distribution of a random sample of *n* observations) for each animal. Theta cycles' amplitudes at baseline were higher in distal than proximal CA1 in trained ($N = 5$) but not in naive animals ($N = 5$). Of note, the average speed of trained and naive rats at baseline was comparable. $^{**}p < 0.010$. Dots, individual D values. Error bars: SEM. All together, these results suggest the absence of "constitutive" proximodistal differences in theta power along CA1 and might indicate a tuning of distal CA1 to the processing of non-spatial (odor) information over time.

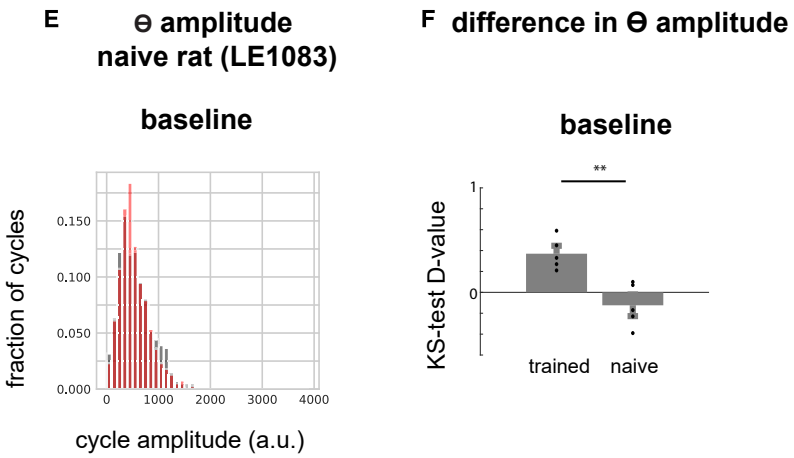

values < 0.010, FDR corrected; see Table S7). Furthermore, this difference was independent of the phase of the task (Friedman's test on Kolmogorov-Smirnov (KS) test D-values (difference of theta amplitudes between distal and proximal CA1) across different task phases: $p = 0.247$; see Figures 4A–4C for examples of theta amplitudes' distribution during the task, Figure S10 for example theta traces, and Tables S7 and S8 for individual theta amplitudes comparison; see STAR Methods for details). Such a proximodistal difference was also observed during free run in trained rats (all *p* values < 0.001, KS test, FDR corrected, Figure 4D; Tables S7 and S8; see results in supplemental information for more analyses on free run). In contrast, amplitudes of theta cycles did not consistently differ between distal and proximal CA1 in naive animals resting in their cage ($n = 5$; Figure 4E; Tables S7 and S8), and a direct comparison between trained and naive animals at baseline established that proximodistal differences were significantly larger in trained than naive animals ($p = 0.008$, Mann-Whitney U test on KS test D-values, Figure 4F; Table S8). Importantly, the average speed of the animals at baseline was comparable between trained and naive rats (1.35 ± 1.18 and 0.99 ± 1.08 cm/s, respectively; two-sample t test, $p = 0.626$, Table S6), indicating that the increase in theta amplitudes in trained rats was unlikely to stem from a difference in the animals' speed.

Altogether, these results suggest a selective enhancement of theta oscillations in distal compared to proximal CA1 in terms of the amplitude of theta cycles in rats that underwent over 2 months of training in the odor memory task used in the present study. In addition, these data reveal the absence of gross "constitutive" differences between the theta oscillations in distal and proximal CA1, suggesting that the enhancement of theta amplitudes in distal CA1 may stem from a selective tuning of this area to the processing of odor, both across and within sessions.

Only the phase locking of CA3 spikes to distal CA1 theta can account for memory performance

To test whether proximodistal differences in the coordination of neuronal spiking and theta oscillations between CA3 and CA1 play an important role in memory retrieval in the present task,

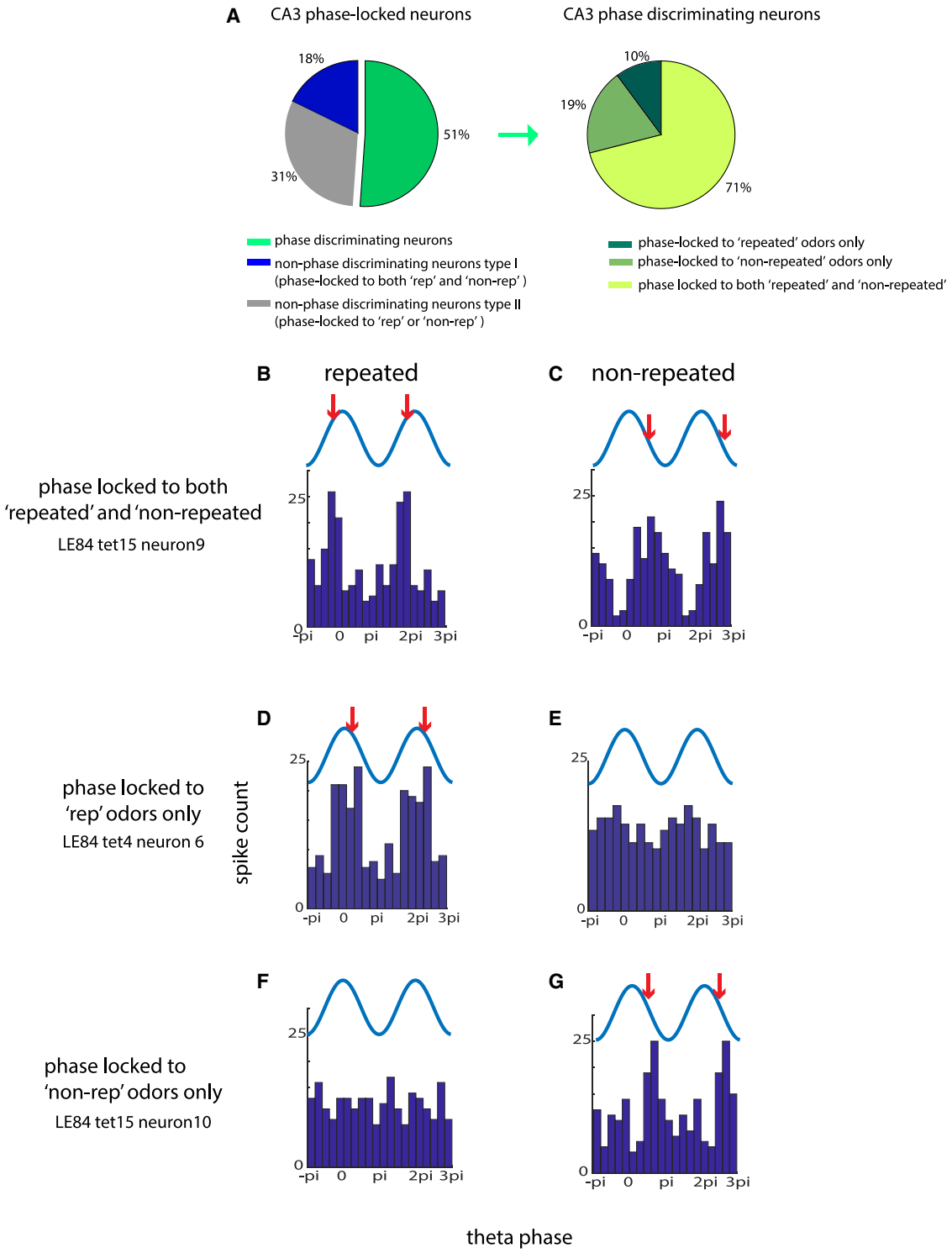

Figure 5. The majority of CA3 spikes are phase locked to distal CA1 theta oscillations during the test phase of this non-spatial memory task

(A) Left, proportion of different types of CA3 neurons phase locked to distal CA1 theta oscillations: the "phase-discriminating neurons" (in green, with a phase-locking angle differing between "repeated" and "non-repeated" odors) and non-phase-discriminating neurons (type I [in blue] and type II [in gray]). Type I neurons were phase locked to the same angle of the theta phase oscillations for repeated and non-repeated odors. Type II were phase locked for only one type of stimulus (gray). About half of the CA3 neurons phase locked to CA1 theta (51%) could discriminate between repeated and non-repeated stimuli—i.e., were phase-discriminating neurons. Right, CA3 phase-discriminating neurons (green on the left) could be subdivided into three groups: the majority of neurons (>70%) were

(legend continued on next page)

we evaluated the proportion of CA3 neurons phase locked to theta oscillations in either distal or proximal CA1. A comparable number of neurons were recorded in proximal and distal CA3 (proxCA3: n = 130; distCA3: n = 109). However, the majority of distCA3 neurons were silent when memory was tested (only 14 out of 109 distCA3 neurons fired more than 20 spikes, while 128 out of 130 proxCA3 neurons fired over this threshold), indirectly supporting our hypothesis that proximal CA3 might be more relevant than distal CA3 for non-spatial information processing.

Analysis on the single-cell level revealed that the vast majority of the CA3 neurons that spiked during the retrieval of both repeated and non-repeated odors were phase locked to distal CA1 theta (135/150; i.e., 90%, 27 per animal on average). For about half of these neurons, the preferred phase-locking angle differed between repeated and non-repeated odors (69/135, i.e., 51%, out of which were 10 effective neurons, 13.8 per animal; Figure 5A left; threshold at $p < 0.050$, circular Watson-Williams multi-sample test for equal variance; see STAR Methods for details). These neurons were termed "phase-discriminating" neurons. Most phase-discriminating neurons were locked to different phases of distal CA1 theta when repeated or non-repeated odors were presented at test (i.e.,71%; 49/69; 9.8 neurons per animal, Figure 5A right; see individual example in Figures 5B and 5C), while the remaining were phase locked to only one of the two stimulus types (non-repeated odors: 19%, 13/69, 2.6 neurons per animal; repeated odors: 10%, 7/69, 1.4 neurons per animal; Figures 5F, 5G, 5D, and 5E, respectively). Similar results were found in relation to the CA3 spikes phase locking to proximal CA1 theta (89% are phase locked; 136/150; 27.2 per animal), among which 46% were phase-discriminating neurons (62/136; 12.4 per animal). In summary, analysis on the single-cell level revealed that the spikes of a similar proportion of CA3 neurons were phase locked to distal or proximal CA1 theta.

At the population level, the analysis of the mean angle of the phase-discriminating CA3 neurons to distal CA1 theta revealed that CA3 neurons tend to fire slightly after the peak of distal CA1 theta (circular mean = 1.5°) only when repeated odors were presented (circular Rayleigh test: repeated, p = 0.017; non-repeated, p = 0.880; Figures 6A and 6B). By contrast, using theta oscillations in proximal CA1 as a reference did not yield any specific patterns for repeated or non-repeated odor retrieval (circular Rayleigh test: repeated: p = 0.700; non-repeated: p = 0.560; Figures 6C and 6D). To compare directly the phase locking of CA3 spikes to distal and proximal CA1 theta for repeated and non-repeated stimuli, we calculated the circular distances of each neuron's mean phase to the circular median of each condition[66] and performed a circular HKtest to compare all conditions at once.[67] This analysis yielded a significant interaction effect between "CA1 theta location" and "stimulus type" ($F_{1,318}$ = 6.150, p = 0.014; circular HKtest). To test if the theta phases of CA3 spikes are more phase locked to distal than proximal CA1 theta during repeated trials (i.e., if the dispersion of the angles is smaller using distal than proximal CA1 theta), we first performed a post hoc analysis on the angular distances to the circular median angles of each dataset.[66] This comparison revealed a significant difference (p = 0.034, FDR corrected; one-tailed Mann-Whitney U test), indicating that CA3 spikes are more phase locked to distal CA1 than to proximal CA1 theta. Second, we examined whether CA3 spikes were more phase locked to distal CA1 theta during repeated than non-repeated trials, i.e., whether the dispersion of the angles is smaller during repeated than non-repeated trials using distal CA1 theta as a reference. This comparison also reached significance (p = 0.046, FDR corrected; one-tailed Mann-Whitney U test on the angular distances to the circular median angles of each dataset), suggesting that CA3 spikes are more phase locked to distal CA1 for repeated than non-repeated stimuli. Altogether these results revealed that CA3 spikes are more phase locked to distal than proximal CA1 theta, only for repeated stimuli, suggesting a selective role of the phase locking of CA3 neurons to distal CA1 theta for retrieving the memory of non-spatial (odor) information.

This result was confirmed by an SVM population analysis showing that the phase information of CA3-discriminating neurons referenced to distal CA1 theta could predict better memory performance trial by trial than the phase information referenced to proximal CA1 (SVM performance: distCA1 89% and proxCA1 49% correct; t tests to chance level: p = 0.001 and p = 0.500, respectively; paired t test between distal and proximal CA1 theta: t_4 = 3.679, p = 0.021; Figure 6E). Hence, these results established that the phase locking of population CA3 spikes to distal CA1 theta is indicative of a prominent role in supporting odor memory retrieval trial by trial when compared to theta phase locking to proximal CA1.

Local spike-theta phase locking in CA3 or CA1 is less critical than cross CA3-CA1 phase locking during the test phase of the task

Subsequently, we evaluated to which extent the coordination of the spiking activity with local theta oscillations in CA3 or CA1 at the population level might contribute to memory retrieval and how this contribution differs from that of the cross-region phase locking.

In CA3, most neurons spiking during the presentation of both repeated and non-repeated odor at test were phase locked to local CA3 theta (theta recorded at the same electrode as the spike; 89%, 133/150, 27 neurons per animal). Over half of the neurons phase locked to local CA3 (53.4%; 71/133, 14.2 neurons per animal) were phase-discriminating neurons (i.e., mean theta phases were different between the presentation of repeated and non-repeated stimuli). No preferred angles were found for the population phase-discriminating CA3 spikes to

phase locked to different phases of distCA1 theta oscillations for repeated and non-repeated odors, while about 20% were phase locked for non-repeated and 10% for repeated stimuli.

(B and C) Phase distributions of representative neurons phase locked to CA1 theta with different angles upon the presentation of repeated and non-repeated odors.

(D and E) Phase locked only repeated odors.

(F and G) Phase locked only for non-repeated odors. Red arrows: mean angle of the population cell firing. "rep," repeated; "non-rep," non-repeated.

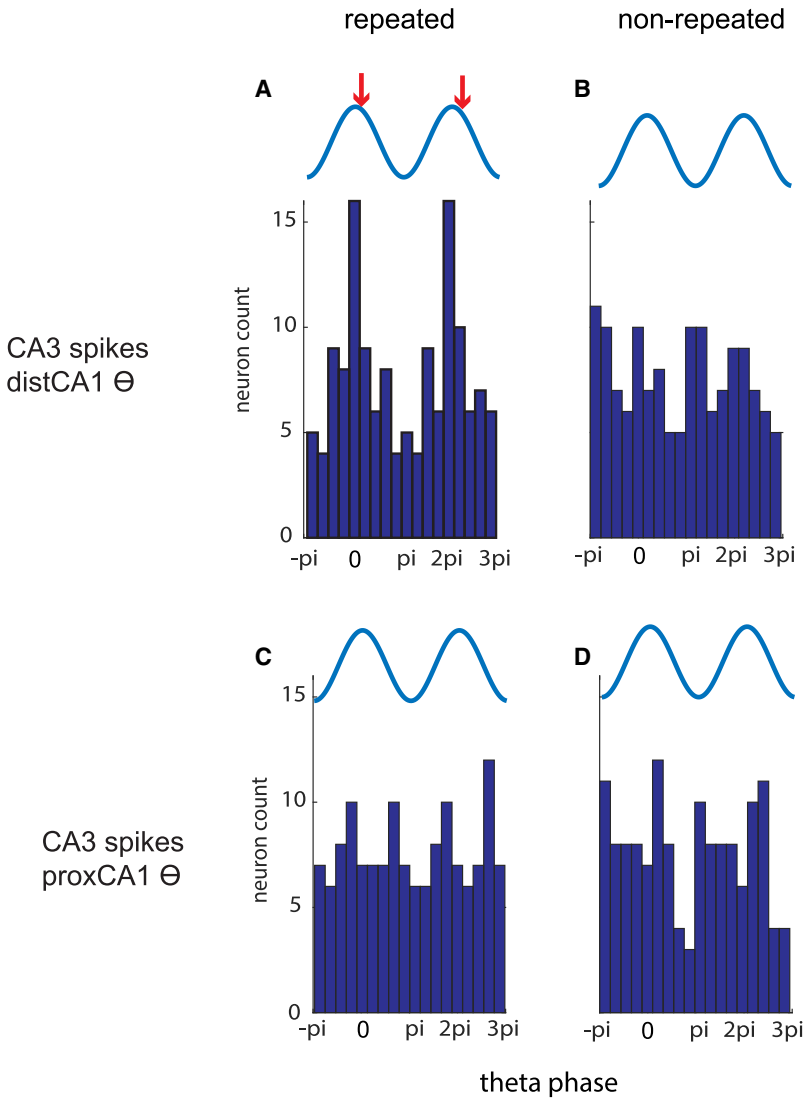

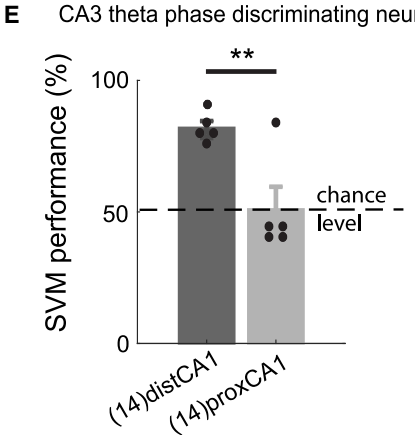

Figure 6. CA3 phase-discriminating neurons are preferentially phase locked close to the peak of distal CA1 theta for experienced ("repeated") odors during the test phase of the task, and classification performance of population CA3 spikes-distal CA1 theta phases predicts memory performance

(A–D) The population distribution of the preferred angle of the theta phases of CA3-discriminating neurons was concentrated close to the peak of theta at test for "repeated" odors when distal CA1 theta was used as a reference (A, mean angle = 0.220, var = 0.758) but not for the presentation of "non-repeated" odors (B, mean angle = −1.300, var = 0.952). No preferred angle was identified when theta in proximal CA1 was used as a reference for either repeated (C, mean angle = −2.492, var = 0.973) or non-repeated (D, mean angle = −2.984, var = 0.898) odors.

(E) SVM classification performances using theta phases of CA3 spikes either referencing to distal CA1 or proximal CA1. The classification performance using the phases of the CA3 neurons referencing to distal CA1 theta, but not to proximal CA1 theta, was above chance level and comparable to memory performance. This indicated that interregional coupling (spike to theta oscillations) between CA3 and CA1 can predict memory performance trial by trial and plays an important role in recognition memory, especially between CA3 and distal CA1 for odor memory. The number of CA3 theta phase discriminating neurons per animal is in brackets. CA3 neurons were recorded along the entire proximodistal axis of CA3. Dots, individual SVM performance; red arrows: mean angle of the population cell firing. Error bars: SEM. $^{**}p < 0.01$.

local CA3 theta oscillations for either odor type (repeated: mean angle = −0.153, $p = 0.061$; non-repeated: mean angle = −1.469, $p = 0.857$; Figures 7A and 7B; circular Rayleigh tests), and the SVM classification performances for CA3 discriminating neurons phase locked to local CA3 theta were low and did not differ significantly from chance level (44% correct, $p = 0.374$, FDR corrected; Figure 7E). Overall, these results suggest that local spike-theta phase locking in CA3 does not critically contribute to memory performance in this task.

In CA1, 93% of the CA1 neurons spiking during both repeated and non-repeated odors at test were phase locked to local CA1 (223/239 neurons, 44.6 neurons per animal) with half of these neurons (49%, 110/223, 22 neurons per animal) being phase-discriminating neurons. Population phase-discriminating CA1 spikes were selectively phase locked close to the peak of local CA1 theta oscillations for the delivery of both repeated and non-repeated odors at test (repeated: mean angle = 0.166, $p = 0.043$; non-repeated: mean angle = −0.304, $p = 0.048$; circular Rayleigh tests; Figures 7C and 7D). However, this phase locking appeared not to be decisive for discriminating repeated from non-repeated odors, as the SVM performance using the CA1 theta phases did not significantly differ from chance level (i.e., 35% correct, $p = 0.058$, FDR corrected; Figure 7E). Hence, similarly to spike-theta phase locking in CA3, these results indicate that local spike-theta phase locking in CA1 does not contribute to a major extent to non-spatial memory performance in the present task.

Furthermore, additional analyses revealed that SVM performance using cross-region phase locking (CA3 spike-distCA1 theta; Figure 6E) was significantly higher than performances obtained using local spike-theta phase locking in CA3 or CA1, indicating that cross-region phase locking might play a more important role than local phase locking in retrieving memories during this task (interaction effect: $F_{2,12} = 29.872$, $p < 0.001$, one-way ANOVA; Tukey-Kramer post hoc comparisons of SVM performances, comparing CA3 spike-distCA1 theta phase performance to local spike-theta phase locking in CA3 or CA1: $t_4 = 8.195$, $p = 0.001$ and $t_4 = 7.526$, $p = 0.002$, respectively, paired t test; no difference between the local spike-theta groups: $p = 0.375$; SVM performance cross-area group: 82% ± 5.70%, SVM local CA1 or CA3 groups: 35% ± 10% and 44% ± 13.42%, respectively).

Altogether, this demonstrates that even when a high proportion of neurons is phase locked to their local theta (the case for both CA1 and CA3), local coordination does not seem to play an essential role in the discrimination between repeated and non-repeated odors on a trial-by-trial basis, further indicating a selective role of the interregional phase locking of CA3 spikes to distal CA1 theta in non-spatial memory retrieval.

DISCUSSION

Our results on theta spike timing in the hippocampus provide insight into the cellular and network mechanisms underlying recognition memory in the hippocampus. We examined theta phase locking of cells within and between hippocampal CA3 and CA1 subregions along the proximodistal axis of the hippocampus and its relationship to memory performance. To do so, we used SVM analyses and a paradigm with a high memory demand often used in humans that was adapted to rats. We found that theta power is high in this odor memory task, similarly to spatially motivated tasks, especially during the test phase of the task. In addition, we observed that the population phase locking of CA3 spikes to CA1 theta, but not local coupling, predicted the memory performance of the animals, which is indicative of an important role of the coordination of CA3 neuronal activity with CA1 theta oscillations in certain non-spatial memory tasks. Importantly, this population phase locking to the peak of CA1 theta was observable only when theta was referred to the distal, but not the proximal part of the CA1 region, suggesting a functional proximodistal gradient along the CA1 axis. In addition, the findings of a higher proportion of effective neurons in distal CA1 and proximal CA3 as well as the fact that only the combined population cell firing of these two areas accounted for memory performance provides further evidence that distal CA1 and proximal CA3 may play an essential role for recognition memory when stimuli are non-spatial.

Theta oscillations are enhanced during non-spatial memory

Many studies investigating spatial navigation and spatial memory have reported modulations of theta oscillations in CA1,[68–73] while much fewer have examined the role of theta range oscillations in memory tasks devoid of salient spatial components.[35–38] In the present study, we report that high theta power is elicited during a non-spatial memory task and modulated by the different epochs of the task. Indeed, our results showed that theta power is high during all phases of the task but was especially strong during the test phase of the task (Figures 3A and 3B).

This result of an enhanced theta power in CA1 during a non-spatial memory task is in line with one of the few studies investigating non-spatial memory in rodents, which, however, focused on intraregional couplings (i.e., did not investigate interregional coupling as in the current study) and used different behavioral tasks (spontaneous object recognition memory and odor-cued delayed nonmatch-to-sample tasks).[1] Our data brought further support to studies in humans reporting a similar pattern in the hippocampus "as a whole,"[35,74–79] showing, for example, that theta oscillations reflect cognitive demands in non-spatial tasks by possibly organizing neural processes through traveling theta waves.[80]

The increase in theta power observed in CA1 at test in our task is unlikely to have stemmed from an increased in locomotor activity as reported during running in previous studies,[21,61–65] because the behavior of the rats during recording bouts was comparable across study and test phases of the task; rats rested during the baseline phase and were virtually stationary for the 2-s bouts following stimulus delivery during the study or the test phases. In addition, we found no general relationship between theta amplitudes and running speed across task phases (see results section and Figure S8). Of note, speed during any phase of the task was lower than 5 cm/s on average, which is in the range of speeds typically excluded from studies reporting a dependency of theta amplitudes and frequency on running speed.[81,82] Hence, the low speed of the animals in the current task might partially explain why our results do not support a strong

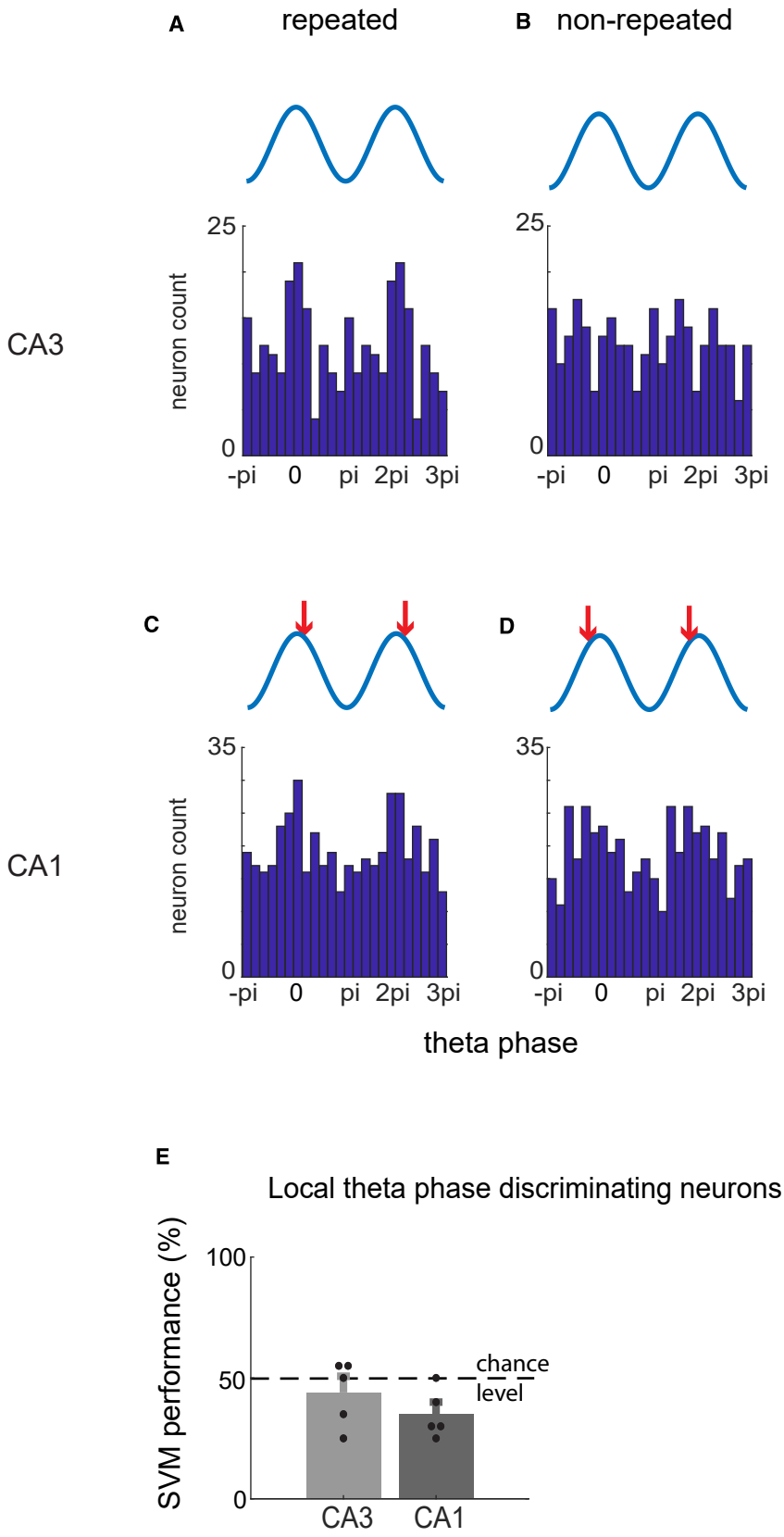

Figure 7. Local spike-theta phase locking in CA1 or CA3 cannot account for the discrimination of "repeated" versus "non-repeated" odors trial by trial

(A–D) Population distribution of the preferred angle of the phases of CA3 spikes for the presentation of "repeated" (A, mean angle = −0.153, var = 0.861) and "non-repeated" (B, mean angle = −1.469, var = 0.968) odors using local theta measured at the same tetrode as the spikes as reference. No preferred angle could be identified for either stimulus type with local CA3 theta as a reference. The population distribution of the phases of CA1 spikes was concentrated close to the peak when local CA1 theta was used as a reference for the presentation of repeated (C, mean angle = 0.166, var = 0.884) as well as non-repeated odors (D, mean angle = −0.304, var = 0.885).

(E) SVM classification performances using either the local CA3 or CA1 spike-theta phases. Neither local CA3 nor CA1 theta phases could predict memory performance above chance level (SVM performance did not differ from chance level). This suggests that intraregional coupling (spike to theta phase) in CA1 or CA3 did not contribute to odor recognition memory to a major extent. Var, variance; dots, individual data; red arrows: mean angle of the population cell firing. Error bars: SEM; chance level: 50%.

dependency of the amplitudes of theta oscillations on running speed. In addition, stress, arousal, and alertness levels, which have also been reported to enhance theta oscillations[83–90] are also unlikely to solely account for the differences observed within animals in the present study. Indeed, stress and arousal levels are expected to be fairly low in our task given that animals have been extensively handled and trained daily for over 2 months, and alertness levels are likely to be comparable during the study and the test phases of the task as, in both cases, rats were left undisturbed 20 min prior to study and test (which corresponds to the baseline and delay period, respectively). Hence, differences in stress, arousal, or alertness levels between epochs are unlikely to account for the differences in theta power observed between the test phase and other phases of the task in CA1 (baseline and study).

Thus, our results point toward a robust role of CA1 theta oscillations in memory function that is independent of the spatial content of the memory.

CA3 spike-CA1 theta coupling predicts successful performance in the present non-spatial memory task

In the present study, we focused on interregional spike-theta coupling, specifically the spike-to-theta phase locking between CA3 and CA1. We showed that the theta phase information of CA3 spikes predicts the memory performance of the animals trial by trial when referenced to the distal but not the proximal part of CA1 in an odor recognition memory task with high memory load (Figure 6). These results complement a handful of studies that have shown intraregional differences in spike-theta phase locking in CA1 at test between studied stimuli (i.e., repeated) and non-experienced (non-repeated) stimuli using either spatial or non-spatial recognition memory tasks with lower memory load such as foraging in environments or spontaneous object/odor recognition.[1,91,92] We additionally investigated interregional spike-to-theta phase locking between CA3 and CA1. The finding that CA3 spikes preferentially phase locked to CA1 theta at the peak of the cycles during the test phase of the task was in line with the prediction of a prevalent computational model suggesting that CA3 inputs should be the strongest at the peak of CA1 theta during retrieval.[1,93] Yet, direct empirical evidence for a preferential phase locking of CA3 neurons to the peak of CA1 theta was missing. Here, we showed that CA3-CA1 coupling indeed takes place shortly after the peak of the theta cycles, bringing clear *in vivo* evidence that CA3 spiking activity and CA1 theta oscillations are coherent at the peak of theta during the test phase of certain memory tasks.

One striking finding in the present study was that the theta phase information of CA3 spikes predicts animals' memory performance only when referred to the distal part of CA1 but not its proximal part. Theta phase could be evaluated reliably across the proximodistal axis of CA1 (see results section and Figure S10). Moreover, this proximodistal difference is unlikely to stem from constitutive differences in the amplitude of theta oscillations between proximal and distal parts of CA1 as no consistent pattern of a proximodistal gradient was found in the 5 naive control rats recorded (i.e., untrained rats; Figure 4E). In contrast, in rats trained on the task, theta power was enhanced in distal CA1 compared to proximal CA1 in all phases of the task as well as during free run (Figures 4A–4D; Table S7). A possible explanation for this enhancement of theta power in trained animals is a progressive tuning of distal CA1 to the processing of non-spatial (odors) information over the 2 months of training. Such a tuning, in terms of increased connectivity between functionally connected cells or brain areas, has been reported in previous studies in humans and rodents upon extensive training.[94–97]

Further evidence for proximodistal gradients along the axis of CA1 and CA3 was found in trained rats in terms of the proportion of effective neurons (i.e., neurons primarily contributing to memory performance in the task; Figures 2E and 2F) and in terms of the population activity of neurons discriminating repeated odors from non-repeated ones (Figure 2B). According to these gradients, spiking activity of distal CA1 and proximal CA3 together best predicted the memory performance. This finding of a preferential involvement of proximal CA3 and distal CA1 in odor memory is in line with recent electrophysiological and immediate-early gene studies reporting a primary contribution of proximal CA3 and distal CA1 to non-spatial (object and odor) information processing or a reduced spatial tuning when compared to distal CA3 and proximal CA1[47–49,51–53]. Importantly, distal CA1 receives extensive neuroanatomical projections from the lateral entorhinal cortex (LEC) and fewer inputs from the medial entorhinal cortex (MEC) in comparison to proximal CA1.[8,10,49,52,98–105] LEC and MEC are also preferentially linked to non-spatial and spatial information processing, respectively.[100,101,106–108] Moreover, in comparison to distal CA3, proximal CA3 receives fewer projections from the spatially tuned enclosed blade of the DG[109–111,112,113] and is also targeted by the exposed blade of the DG, which is not engaged by spatial experience and more involved in odor discrimination than the enclosed blade.[110,114] Altogether, these results point toward the existence of a non-spatial medial temporal lobe subnetwork including the exposed blade of DG, proximal CA3, distal CA1, and the LEC.[47,51] In the current study, we provide *in vivo* evidence for a functional interaction between the hippocampal subregions of this network, with a preferential recruitment of proximal CA3 and distal CA1 during the test phase of a non-spatial memory task. In addition, we demonstrate that these areas have important interregional functional processing as CA3 spike-distal CA1 theta coupling best predicts memory performance in our task.

Importantly, it cannot be entirely ruled out that the synchronization of CA3 neuronal firing with CA1 theta oscillations might, to some degree, reflect the influence of EC theta activity, given the substantial inputs of EC to CA1 and the high coherence between CA1 and EC theta.[13,115–118] However, our study reveals a discernible gradient in theta power along the proximodistal axis of CA1, and notably, only the phase locking of CA3 spikes to distal CA1 theta (not to proximal CA1 theta) could reliably predict memory performance. This suggests that theta oscillations in CA1 may be subjected to modulation by local circuitry to a greater extent than originally described.[118,119] Consequently, it becomes less plausible that EC theta oscillations play an important role in the observed phase locking of CA3 activity. In addition, the identification of a strong inhibitory projection from CA1 to CA3[120] and the report of a causal influence from CA1 to CA3 in a study with simultaneous spiking recording[121] further

support a possible entrainment of CA3 spikes by CA1 theta oscillations. Other intra- and extra-hippocampal theta oscillations propagated by volume conduction have been suggested to contribute to hippocampal theta oscillations[15,122–124] and the "rhythmicity" of these oscillations to differ across task phases during learning for some of the generators.[125] Hence, it also cannot be entirely excluded that volume conduction could contribute to the differences reported in the present study. However, our results showed that the theta phase information of CA3 spikes using proximal CA1 or local CA3 theta oscillations as references cannot predict memory performance as well as using distal CA1 theta (Figures 6E and 7E), suggesting that the propagation by volume conduction of theta oscillations emerging from these generators (proximal CA1 or local CA3) may not contribute to a major extent.

In contrast to the interregional spike-theta phase locking between CA3 and CA1, local coupling in CA1 or CA3 failed to reveal a strong relationship with memory performance, even though the local spike-theta phase locking in CA1 or CA3 was found to be important in tasks involving spatial navigation.[1,14,24,126–131] However, our results are consistent with the handful of studies that use non-spatial stimuli and report that even though most cells exhibit significant spike-theta phase locking locally, there is no significant relationship between local spike-theta phase locking and memory performance.[132,133] Hence, our results suggest that intra- and interregional spike-theta coherence might serve vastly different purposes in odor recognition memory. Finally, in line with recent studies showing that discrimination between stimuli was better predicted by population level analysis as opposed to individual cell firing,[20,56,57] no specific pattern of increased or decreased firing rates was detected at the single-cell level (Figure S5). This, together with our finding that the combination of population activity can discriminate repeated from non-repeated odors, suggests that differences in population firing between stimulus types might serve as an underlying mechanism for recognition memory rather than a general enhancement or suppression of individual cell firing rates.

Limitations of the study

It should be noted that given the experimental design of the task (i.e., training animals over 2 months to a plateau of 80% correct responses on average), the high ratio of correct versus incorrect trials does not allow us to assert that the mechanism described in the present study is exclusively at play for successful memory retrieval (i.e., that it pertains only to correct and not to incorrect trials). In a similar line, because of this low number of error trials, the extent to which this mechanism contributes to specific behavioral combinations (correct responses: repeated odor-turn or non-repeated odor-dig; incorrect responses: repeated odor-dig or non-repeated odor-turn) was not studied. Indeed, the 1–2 incorrect trials performed during a session (for repeated and non-repeated stimuli) contain 5 to 20 spikes, which is too low to enable a reliable estimation of spike-theta coherence.[130] In addition, the present study does not investigate whether differential neural responses might predict subsequent behavioral responses.

As a general conclusion, we showed here that theta oscillations play an important role in non-spatial memory, as is the case for spatial navigation and memory. In addition, our results indicate that interregional synchronization of neuronal spiking with theta oscillations, especially between CA3 and distal CA1 and in the case of non-spatial memory, might facilitate discriminative processes tied to memory function. Moreover, our findings complemented previous theoretical and empirical studies by providing clear evidence that the population of CA3 neurons does fire close to the peak of CA1 theta cycles during successful recognition memory. In contrast, similar coupling at the local level in CA1 or CA3 as well as rate or phase coding at the single-cell level appeared to play less of a decisive role in recognition memory.

STAR★METHODS

Detailed methods are provided in the online version of this paper and include the following:

- KEY RESOURCES TABLE
- RESOURCE AVAILABILITY
  - Lead contact
  - Materials availability
  - Data and code availability
- EXPERIMENTAL MODEL AND STUDY PARTICIPANT DETAILS
  - Animals
- METHOD DETAILS
  - Surgery
  - Behavioral stimuli
  - Behavioral paradigm and training
  - Histology and reconstruction of recording positions
  - Data acquisition
- QUANTIFICATION AND STATISTICAL ANALYSIS
  - Behavior
  - Spike sorting
  - Support vector machine (SVM)
  - Selection of 'effective' neurons
  - Analyses
  - Generalized linear mixed effect (GLME) model
  - Statistical analysis

SUPPLEMENTAL INFORMATION

Supplemental information can be found online at https://doi.org/10.1016/j.celrep.2024.114276.

ACKNOWLEDGMENTS

We would like to thank J. Maiwald for her assistance in animal behavior training, experiments, and brain slice preparation; D. Koch for her assistance in recording drive building and brain slicing; K. Kaefer and J. Wallenschus (IST Austria) for their initial technical support; S. Mikulovich for her comments on an early version of the manuscript; C. Reichert for his comments on SVM analyses; and J. Pakan for English proofreading. This project is funded by the DFG (CRC 779 and CRC 1436).

AUTHOR CONTRIBUTIONS

S.-P.K. and M.M.S. designed the experiments; S.-P.K. and E.A. conducted the experiments; S.-P.K. and N.A. analyzed the data with feedback from J.C., M.M.S., and M.Y.; H.M.-O. performed DeepLabCut analyses; S.-P.K. and M.M.S. wrote and J.C., M.Y., and R.K. edited the manuscript. M.M.S. is corresponding for the conceptual and mechanistic framework underlying the design of the experiments; S.-P.K. is corresponding for the formulation and identification of the electrophysiological mechanisms.

DECLARATION OF INTERESTS

The authors declare no competing interests.

Received: June 9, 2022
Revised: January 9, 2024
Accepted: May 9, 2024

REFERENCES

1. Manns, J.R., Zilli, E.A., Ong, K.C., Hasselmo, M.E., and Eichenbaum, H. (2007). Hippocampal CA1 spiking during encoding and retrieval: relation to theta phase. Neurobiol. Learn. Mem. *87*, 9–20. https://doi.org/10.1016/j.nlm.2006.05.007.
2. Koen, J.D., and Yonelinas, A.P. (2014). The effects of healthy aging, amnestic mild cognitive impairment, and Alzheimer's disease on recollection and familiarity: a meta-analytic review. Neuropsychol. Rev. *24*, 332–354. https://doi.org/10.1007/s11065-014-9266-5.
3. Scoville, W.B., and Milner, B. (1957). Loss of recent memory after bilateral hippocampal lesions. J. Neurol. Neurosurg. Psychiatry *20*, 11–21. https://doi.org/10.1136/jnnp.20.1.11.
4. Kaada, B., Rasmussen, E.W., and Kveim, O. (1961). Effects of hippocampal lesions on maze learning and retention in rats. Exp. Neurol. *3*, 333–355. https://doi.org/10.1016/0014-4886(61)90009-7.
5. Yonelinas, A.P., Aly, M., Wang, W.-C., and Koen, J.D. (2010). Recollection and familiarity: examining controversial assumptions and new directions. Hippocampus *20*, 1178–1194. https://doi.org/10.1002/hipo.20864.
6. Eichenbaum, H., Yonelinas, A.P., and Ranganath, C. (2007). The medial temporal lobe and recognition memory. Annu. Rev. Neurosci. *30*, 123–153. https://doi.org/10.1146/annurev.neuro.30.051606.094328.
7. Zola-Morgan, S., Squire, L.R., and Mishkin, M. (1982). The neuroanatomy of amnesia: amygdala-hippocampus versus temporal stem. Science *218*, 1337–1339. https://doi.org/10.1126/science.6890713.
8. Amaral, D.G., and Witter, M.P. (1989). The three-dimensional organization of the hippocampal formation: a review of anatomical data. Neuroscience *31*, 571–591. https://doi.org/10.1016/0306-4522(89)90424-7.
9. Amaral, D.G. (1993). Emerging principles of intrinsic hippocampal organization. Curr. Opin. Neurobiol. *3*, 225–229. https://doi.org/10.1016/0959-4388(93)90214-j.
10. Ishizuka, N., Weber, J., and Amaral, D.G. (1990). Organization of intrahippocampal projections originating from CA3 pyramidal cells in the rat. J. Comp. Neurol. *295*, 580–623. https://doi.org/10.1002/cne.902950407.
11. Brivanlou, I.H., Dantzker, J.L.M., Stevens, C.F., and Callaway, E.M. (2004). Topographic specificity of functional connections from hippocampal CA3 to CA1. Proc. Natl. Acad. Sci. USA *101*, 2560–2565. https://doi.org/10.1073/pnas.0308577100.
12. van Strien, N.M., Cappaert, N.L.M., and Witter, M.P. (2009). The anatomy of memory: an interactive overview of the parahippocampal-hippocampal network. Nat. Rev. Neurosci. *10*, 272–282. https://doi.org/10.1038/nrn2614.
13. Zutshi, I., Valero, M., Fernandez-Ruiz, A., and Buzsaki, G. (2022). Extrinsic control and intrinsic computation in the hippocampal CA1 circuit. Neuron *110*, 658–673.e655. https://doi.org/10.1016/j.neuron.2021.11.015.
14. Fernandez-Ruiz, A., Oliva, A., Nagy, G.A., Maurer, A.P., Berenyi, A., and Buzsaki, G. (2017). Entorhinal-CA3 Dual-Input Control of Spike Timing in the Hippocampus by Theta-Gamma Coupling. Neuron *93*, 1213–1226.e1215. https://doi.org/10.1016/j.neuron.2017.02.017.
15. Schomburg, E.W., Fernández-Ruiz, A., Mizuseki, K., Berényi, A., Anastassiou, C.A., Koch, C., and Buzsáki, G. (2014). Theta phase segregation of input-specific gamma patterns in entorhinal-hippocampal networks. Neuron *84*, 470–485. https://doi.org/10.1016/j.neuron.2014.08.051.
16. Montgomery, S.M., Sirota, A., and Buzsáki, G. (2008). Theta and gamma coordination of hippocampal networks during waking and rapid eye movement sleep. J. Neurosci. *28*, 6731–6741. https://doi.org/10.1523/JNEUROSCI.1227-08.2008.
17. Dragoi, G., Carpi, D., Recce, M., Csicsvari, J., and Buzsáki, G. (1999). Interactions between hippocampus and medial septum during sharp waves and theta oscillation in the behaving rat. J. Neurosci. *19*, 6191–6199.
18. Colgin, L.L., Denninger, T., Fyhn, M., Hafting, T., Bonnevie, T., Jensen, O., Moser, M.B., and Moser, E.I. (2009). Frequency of gamma oscillations routes flow of information in the hippocampus. Nature *462*, 353–357. https://doi.org/10.1038/nature08573.
19. Zheng, C., Bieri, K.W., Hwaun, E., and Colgin, L.L. (2016). Fast Gamma Rhythms in the Hippocampus Promote Encoding of Novel Object-Place Pairings. eNeuro *3*. https://doi.org/10.1523/ENEURO.0001-16.2016.
20. El-Gaby, M., Reeve, H.M., Lopes-Dos-Santos, V., Campo-Urriza, N., Perestenko, P.V., Morley, A., Strickland, L.A.M., Lukács, I.P., Paulsen, O., and Dupret, D. (2021). An emergent neural coactivity code for dynamic memory. Nat. Neurosci. *24*, 694–704. https://doi.org/10.1038/s41593-021-00820-w.
21. Buzsaki, G., and Moser, E.I. (2013). Memory, navigation and theta rhythm in the hippocampal-entorhinal system. Nat. Neurosci. *16*, 130–138. https://doi.org/10.1038/nn.3304.
22. Buzsaki, G. (2005). Theta rhythm of navigation: link between path integration and landmark navigation, episodic and semantic memory. Hippocampus *15*, 827–840. https://doi.org/10.1002/hipo.20113.
23. Skaggs, W.E., McNaughton, B.L., Wilson, M.A., and Barnes, C.A. (1996). Theta phase precession in hippocampal neuronal populations and the compression of temporal sequences. Hippocampus *6*, 149–172. https://doi.org/10.1002/(SICI)1098-1063(1996)6:2<149::AID-HIPO6>3.0.CO;2-K.
24. Dragoi, G., and Buzsáki, G. (2006). Temporal encoding of place sequences by hippocampal cell assemblies. Neuron *50*, 145–157. https://doi.org/10.1016/j.neuron.2006.02.023.
25. Colgin, L.L. (2013). Mechanisms and functions of theta rhythms. Annu. Rev. Neurosci. *36*, 295–312. https://doi.org/10.1146/annurev-neuro-062012-170330.
26. Burgess, N., and O'Keefe, J. (2011). Models of place and grid cell firing and theta rhythmicity. Curr. Opin. Neurobiol. *21*, 734–744. https://doi.org/10.1016/j.conb.2011.07.002.
27. Harris, K.D., Henze, D.A., Hirase, H., Leinekugel, X., Dragoi, G., Czurkó, A., and Buzsáki, G. (2002). Spike train dynamics predicts theta-related phase precession in hippocampal pyramidal cells. Nature *417*, 738–741. https://doi.org/10.1038/nature00808.
28. Benchenane, K., Peyrache, A., Khamassi, M., Tierney, P.L., Gioanni, Y., Battaglia, F.P., and Wiener, S.I. (2010). Coherent theta oscillations and reorganization of spike timing in the hippocampal- prefrontal network upon learning. Neuron *66*, 921–936. https://doi.org/10.1016/j.neuron.2010.05.013.
29. Hyman, J.M., Zilli, E.A., Paley, A.M., and Hasselmo, M.E. (2010). Working Memory Performance Correlates with Prefrontal-Hippocampal Theta Interactions but not with Prefrontal Neuron Firing Rates. Front. Integr. Neurosci. *4*, 2. https://doi.org/10.3389/neuro.07.002.2010.
30. Ishino, S., Takahashi, S., Ogawa, M., and Sakurai, Y. (2017). Hippocampal-prefrontal theta phase synchrony in planning of multi-step actions based on memory retrieval. Eur. J. Neurosci. *45*, 1313–1324. https://doi.org/10.1111/ejn.13547.
31. Siapas, A.G., Lubenov, E.V., and Wilson, M.A. (2005). Prefrontal phase locking to hippocampal theta oscillations. Neuron *46*, 141–151. https://doi.org/10.1016/j.neuron.2005.02.028.

32. Wirt, R.A., and Hyman, J.M. (2019). ACC Theta Improves Hippocampal Contextual Processing during Remote Recall. Cell Rep. *27*, 2313–2327.e4. https://doi.org/10.1016/j.celrep.2019.04.080.

33. Mizuseki, K., Sirota, A., Pastalkova, E., and Buzsáki, G. (2009). Theta oscillations provide temporal windows for local circuit computation in the entorhinal-hippocampal loop. Neuron *64*, 267–280. https://doi.org/10.1016/j.neuron.2009.08.037.

34. Frank, L.M., Brown, E.N., and Wilson, M.A. (2001). A comparison of the firing properties of putative excitatory and inhibitory neurons from CA1 and the entorhinal cortex. J. Neurophysiol. *86*, 2029–2040. https://doi.org/10.1152/jn.2001.86.4.2029.

35. Pacheco Estefan, D., Zucca, R., Arsiwalla, X., Principe, A., Zhang, H., Rocamora, R., Axmacher, N., and Verschure, P.F.M.J. (2021). Volitional learning promotes theta phase coding in the human hippocampus. Proc. Natl. Acad. Sci. USA *118*, e2021238118. https://doi.org/10.1073/pnas.2021238118.

36. Leszczynski, M., Fell, J., and Axmacher, N. (2015). Rhythmic Working Memory Activation in the Human Hippocampus. Cell Rep. *13*, 1272–1282. https://doi.org/10.1016/j.celrep.2015.09.081.

37. Axmacher, N., Henseler, M.M., Jensen, O., Weinreich, I., Elger, C.E., and Fell, J. (2010). Cross-frequency coupling supports multi-item working memory in the human hippocampus. Proc. Natl. Acad. Sci. USA *107*, 3228–3233. https://doi.org/10.1073/pnas.0911531107.

38. Canolty, R.T., Edwards, E., Dalal, S.S., Soltani, M., Nagarajan, S.S., Kirsch, H.E., Berger, M.S., Barbaro, N.M., and Knight, R.T. (2006). High gamma power is phase-locked to theta oscillations in human neocortex. Science *313*, 1626–1628. https://doi.org/10.1126/science.1128115.

39. Buzsaki, G., and Eidelberg, E. (1983). Phase relations of hippocampal projection cells and interneurons to theta activity in the anesthetized rat. Brain Res. *266*, 334–339. https://doi.org/10.1016/0006-8993(83)90665-0.

40. Fox, S.E., Wolfson, S., and Ranck, J.B., Jr. (1986). Hippocampal theta rhythm and the firing of neurons in walking and urethane anesthetized rats. Exp. Brain Res. *62*, 495–508. https://doi.org/10.1007/BF00236028.

41. Harris, K.D., Csicsvari, J., Hirase, H., Dragoi, G., and Buzsáki, G. (2003). Organization of cell assemblies in the hippocampus. Nature *424*, 552–556. https://doi.org/10.1038/nature01834.

42. Buzsaki, G., and Tingley, D. (2018). Space and Time: The Hippocampus as a Sequence Generator. Trends Cognit. Sci. *22*, 853–869. https://doi.org/10.1016/j.tics.2018.07.006.

43. Radvansky, G.A. (2006). Human Memory (Pearson/Allyn and Bacon).

44. Yonelinas, A.P. (1997). Recognition memory ROCs for item and associative information: the contribution of recollection and familiarity. Mem. Cognit. *25*, 747–763. https://doi.org/10.3758/bf03211318.

45. Wixted, J.T., Goldinger, S.D., Squire, L.R., Kuhn, J.R., Papesh, M.H., Smith, K.A., Treiman, D.M., and Steinmetz, P.N. (2018). Coding of episodic memory in the human hippocampus. Proc. Natl. Acad. Sci. USA *115*, 1093–1098. https://doi.org/10.1073/pnas.1716443115.

46. Stark, C.E., and Squire, L.R. (2000). Functional magnetic resonance imaging (fMRI) activity in the hippocampal region during recognition memory. J. Neurosci. *20*, 7776–7781.

47. Beer, Z., Vavra, P., Atucha, E., Rentzing, K., Heinze, H.J., and Sauvage, M.M. (2018). The memory for time and space differentially engages the proximal and distal parts of the hippocampal subfields CA1 and CA3. PLoS Biol. *16*, e2006100. https://doi.org/10.1371/journal.pbio.2006100.

48. Flasbeck, V., Atucha, E., Nakamura, N.H., Yoshida, M., and Sauvage, M.M. (2018). Spatial information is preferentially processed by the distal part of CA3: Implication for memory retrieval. Behav. Brain Res. *354*, 31–38. https://doi.org/10.1016/j.bbr.2018.07.023.

49. Henriksen, E.J., Colgin, L.L., Barnes, C.A., Witter, M.P., Moser, M.B., and Moser, E.I. (2010). Spatial representation along the proximodistal axis of CA1. Neuron *68*, 127–137. https://doi.org/10.1016/j.neuron.2010.08.042.

50. Lu, L., Igarashi, K.M., Witter, M.P., Moser, E.I., and Moser, M.B. (2015). Topography of Place Maps along the CA3-to-CA2 Axis of the Hippocampus. Neuron *87*, 1078–1092. https://doi.org/10.1016/j.neuron.2015.07.007.

51. Nakamura, N.H., Flasbeck, V., Maingret, N., Kitsukawa, T., and Sauvage, M.M. (2013). Proximodistal segregation of nonspatial information in CA3: preferential recruitment of a proximal CA3-distal CA1 network in nonspatial recognition memory. J. Neurosci. *33*, 11506–11514. https://doi.org/10.1523/JNEUROSCI.4480-12.2013.

52. Burke, S.N., Maurer, A.P., Nematollahi, S., Uprety, A.R., Wallace, J.L., and Barnes, C.A. (2011). The influence of objects on place field expression and size in distal hippocampal CA1. Hippocampus *21*, 783–801. https://doi.org/10.1002/hipo.20929.

53. Vandrey, B., Duncan, S., and Ainge, J.A. (2021). Object and object-memory representations across the proximodistal axis of CA1. Hippocampus *31*, 881–896. https://doi.org/10.1002/hipo.23331.

54. Fortin, N.J., Wright, S.P., and Eichenbaum, H. (2004). Recollection-like memory retrieval in rats is dependent on the hippocampus. Nature *431*, 188–191. https://doi.org/10.1038/nature02853.

55. Sauvage, M.M., Beer, Z., Ekovich, M., Ho, L., and Eichenbaum, H. (2010). The caudal medial entorhinal cortex: a selective role in recollection-based recognition memory. J. Neurosci. *30*, 15695–15699. https://doi.org/10.1523/JNEUROSCI.4301-10.2010.

56. Guzowski, J.F., Knierim, J.J., and Moser, E.I. (2004). Ensemble dynamics of hippocampal regions CA3 and CA1. Neuron *44*, 581–584. https://doi.org/10.1016/j.neuron.2004.11.003.

57. Leutgeb, S., Leutgeb, J.K., Treves, A., Moser, M.B., and Moser, E.I. (2004). Distinct ensemble codes in hippocampal areas CA3 and CA1. Science *305*, 1295–1298. https://doi.org/10.1126/science.1100265.

58. Ku, S.P., Gretton, A., Macke, J., and Logothetis, N.K. (2008). Comparison of pattern recognition methods in classifying high-resolution BOLD signals obtained at high magnetic field in monkeys. Magn. Reson. Imaging *26*, 1007–1014. https://doi.org/10.1016/j.mri.2008.02.016.

59. Brinkmann, B.H., Patterson, E.E., Vite, C., Vasoli, V.M., Crepeau, D., Stead, M., Howbert, J.J., Cherkassky, V., Wagenaar, J.B., Litt, B., and Worrell, G.A. (2015). Forecasting Seizures Using Intracranial EEG Measures and SVM in Naturally Occurring Canine Epilepsy. PLoS One *10*, e0133900. https://doi.org/10.1371/journal.pone.0133900.

60. Cole, S., and Voytek, B. (2019). Cycle-by-cycle analysis of neural oscillations. J. Neurophysiol. *122*, 849–861. https://doi.org/10.1152/jn.00273.2019.

61. Korotkova, T., Ponomarenko, A., Monaghan, C.K., Poulter, S.L., Cacucci, F., Wills, T., Hasselmo, M.E., and Lever, C. (2018). Reconciling the different faces of hippocampal theta: The role of theta oscillations in cognitive, emotional and innate behaviors. Neurosci. Biobehav. Rev. *85*, 65–80. https://doi.org/10.1016/j.neubiorev.2017.09.004.

62. McFarland, W.L., Teitelbaum, H., and Hedges, E.K. (1975). Relationship between hippocampal theta activity and running speed in the rat. J. Comp. Physiol. Psychol. *88*, 324–328. https://doi.org/10.1037/h0076177.

63. Buzsaki, G., Rappelsberger, P., and Kellenyi, L. (1985). Depth profiles of hippocampal rhythmic slow activity ('theta rhythm') depend on behaviour. Electroencephalogr. Clin. Neurophysiol. *61*, 77–88. https://doi.org/10.1016/0013-4694(85)91075-2.

64. Buzsaki, G., Grastyan, E., Czopf, J., Kellenyi, L., and Prohaska, O. (1981). Changes in neuronal transmission in the rat hippocampus during behavior. Brain Res. *225*, 235–247. https://doi.org/10.1016/0006-8993(81)90833-7.

65. McClain, K., Tingley, D., Heeger, D.J., and Buzsáki, G. (2019). Position-theta-phase model of hippocampal place cell activity applied to quantification of running speed modulation of firing rate. Proc. Natl. Acad. Sci. USA *116*, 27035–27042. https://doi.org/10.1073/pnas.1912792116.

66. Zar, J.H. (1999). Biostatistical Analysis, 4th Edition (Prentice Hall Saddle River).

67. Harrison, D., and Kanji, G.K. (1988). The development of analysis of variance for circular data. J. Appl. Stat. *15*, 197–223. https://doi.org/10.1080/02664768800000026.

68. Whishaw, I.Q., and Vanderwolf, C.H. (1973). Hippocampal EEG and behavior: changes in amplitude and frequency of RSA (theta rhythm) associated with spontaneous and learned movement patterns in rats and cats. Behav. Biol. *8*, 461–484. https://doi.org/10.1016/s0091-6773(73)80041-0.

69. Wyble, B.P., Hyman, J.M., Rossi, C.A., and Hasselmo, M.E. (2004). Analysis of theta power in hippocampal EEG during bar pressing and running behavior in rats during distinct behavioral contexts. Hippocampus *14*, 662–674. https://doi.org/10.1002/hipo.20012.

70. Terrazas, A., Krause, M., Lipa, P., Gothard, K.M., Barnes, C.A., and McNaughton, B.L. (2005). Self-motion and the hippocampal spatial metric. J. Neurosci. *25*, 8085–8096. https://doi.org/10.1523/JNEUROSCI.0693-05.2005.

71. Kunz, L., Maidenbaum, S., Chen, D., Wang, L., Jacobs, J., and Axmacher, N. (2019). Mesoscopic Neural Representations in Spatial Navigation. Trends Cogn. Sci. *23*, 615–630. https://doi.org/10.1016/j.tics.2019.04.011.

72. Hoffmann, L.C., Cicchese, J.J., and Berry, S.D. (2015). Harnessing the power of theta: natural manipulations of cognitive performance during hippocampal theta-contingent eyeblink conditioning. Front. Syst. Neurosci. *9*, 50. https://doi.org/10.3389/fnsys.2015.00050.

73. Petersen, P.C., and Buzsaki, G. (2020). Cooling of Medial Septum Reveals Theta Phase Lag Coordination of Hippocampal Cell Assemblies. Neuron *107*, 731–744.e733. https://doi.org/10.1016/j.neuron.2020.05.023.

74. Cohen, N., Pell, L., Edelson, M.G., Ben-Yakov, A., Pine, A., and Dudai, Y. (2015). Peri-encoding predictors of memory encoding and consolidation. Neurosci. Biobehav. Rev. *50*, 128–142. https://doi.org/10.1016/j.neubiorev.2014.11.002.

75. Klimesch, W. (1999). EEG alpha and theta oscillations reflect cognitive and memory performance: a review and analysis. Brain Res. Brain Res. Rev. *29*, 169–195. https://doi.org/10.1016/s0165-0173(98)00056-3.

76. Vulic, K., Bjekic, J., Paunovic, D., Jovanovic, M., Milanovic, S., and Filipovic, S.R. (2021). Theta-modulated oscillatory transcranial direct current stimulation over posterior parietal cortex improves associative memory. Sci. Rep. *11*, 3013. https://doi.org/10.1038/s41598-021-82577-7.

77. Kragel, J.E., Schuele, S., VanHaerents, S., Rosenow, J.M., and Voss, J.L. (2021). Rapid coordination of effective learning by the human hippocampus. Sci. Adv. *7*, eabf7144. https://doi.org/10.1126/sciadv.abf7144.

78. Tambini, A., Nee, D.E., and D'Esposito, M. (2018). Hippocampal-targeted Theta-burst Stimulation Enhances Associative Memory Formation. J. Cognit. Neurosci. *30*, 1452–1472. https://doi.org/10.1162/jocn_a_01300.

79. Hebscher, M., Kragel, J.E., Kahnt, T., and Voss, J.L. (2021). Enhanced reinstatement of naturalistic event memories due to hippocampal-network-targeted stimulation. Curr. Biol. *31*, 1428–1437.e5. https://doi.org/10.1016/j.cub.2021.01.027.

80. Zhang, H., Watrous, A.J., Patel, A., and Jacobs, J. (2018). Theta and Alpha Oscillations Are Traveling Waves in the Human Neocortex. Neuron *98*, 1269–1281.e4. https://doi.org/10.1016/j.neuron.2018.05.019.

81. Kaefer, K., Nardin, M., Blahna, K., and Csicsvari, J. (2020). Replay of Behavioral Sequences in the Medial Prefrontal Cortex during Rule Switching. Neuron *106*, 154–165.e6. https://doi.org/10.1016/j.neuron.2020.01.015.

82. Stella, F., Baracskay, P., O'Neill, J., and Csicsvari, J. (2019). Hippocampal Reactivation of Random Trajectories Resembling Brownian Diffusion. Neuron *102*, 450–461.e457. https://doi.org/10.1016/j.neuron.2019.01.052.

83. Mikulovic, S., Restrepo, C.E., Siwani, S., Bauer, P., Pupe, S., Tort, A.B.L., Kullander, K., and Leão, R.N. (2018). Ventral hippocampal OLM cells control type 2 theta oscillations and response to predator odor. Nat. Commun. *9*, 3638. https://doi.org/10.1038/s41467-018-05907-w.

84. Hata, T., Nishimura, Y., Kita, T., Kawabata, A., and Itoh, E. (1987). Electrocorticogram in rats loaded with SART stress (repeated cold stress). Jpn. J. Pharmacol. *45*, 365–372. https://doi.org/10.1254/jjp.45.365.

85. Yamamoto, J. (1998). Relationship between hippocampal theta-wave frequency and emotional behaviors in rabbits produced with stresses or psychotropic drugs. Jpn. J. Pharmacol. *76*, 125–127. https://doi.org/10.1254/jjp.76.125.

86. Chang, F.C. (1992). Modification of medullary respiratory-related discharge patterns by behaviors and states of arousal. Brain Res. *571*, 281–292. https://doi.org/10.1016/0006-8993(92)90666-w.

87. Nollet, M., Hicks, H., McCarthy, A.P., Wu, H., Möller-Levet, C.S., Laing, E.E., Malki, K., Lawless, N., Wafford, K.A., Dijk, D.J., and Winsky-Sommerer, R. (2019). REM sleep's unique associations with corticosterone regulation, apoptotic pathways, and behavior in chronic stress in mice. Proc. Natl. Acad. Sci. USA *116*, 2733–2742. https://doi.org/10.1073/pnas.1816456116.

88. Murthy, S., Kane, G.A., Katchur, N.J., Lara Mejia, P.S., Obiofuma, G., Buschman, T.J., McEwen, B.S., and Gould, E. (2019). Perineuronal Nets, Inhibitory Interneurons, and Anxiety-Related Ventral Hippocampal Neuronal Oscillations Are Altered by Early Life Adversity. Biol. Psychiatr. *85*, 1011–1020. https://doi.org/10.1016/j.biopsych.2019.02.021.

89. Shors, T.J., Gallegos, R.A., and Breindl, A. (1997). Transient and persistent consequences of acute stress on long-term potentiation (LTP), synaptic efficacy, theta rhythms and bursts in area CA1 of the hippocampus. Synapse *26*, 209–217. https://doi.org/10.1002/(SICI)1098-2396(199707)26:3<209::AID-SYN2>3.0.CO;2-B.

90. Liberman, T., Velluti, R.A., and Pedemonte, M. (2009). Temporal correlation between auditory neurons and the hippocampal theta rhythm induced by novel stimulations in awake guinea pigs. Brain Res. *1298*, 70–77. https://doi.org/10.1016/j.brainres.2009.08.061.

91. Lever, C., Burton, S., Jeewajee, A., Wills, T.J., Cacucci, F., Burgess, N., and O'Keefe, J. (2010). Environmental novelty elicits a later theta phase of firing in CA1 but not subiculum. Hippocampus *20*, 229–234. https://doi.org/10.1002/hipo.20671.

92. Douchamps, V., Jeewajee, A., Blundell, P., Burgess, N., and Lever, C. (2013). Evidence for encoding versus retrieval scheduling in the hippocampus by theta phase and acetylcholine. J. Neurosci. *33*, 8689–8704. https://doi.org/10.1523/JNEUROSCI.4483-12.2013.

93. Hasselmo, M.E., Bodelón, C., and Wyble, B.P. (2002). A proposed function for hippocampal theta rhythm: separate phases of encoding and retrieval enhance reversal of prior learning. Neural Comput. *14*, 793–817. https://doi.org/10.1162/089976602317318965.

94. Olofsson, J.A.-O., Zhou, G., East, B.S., Zelano, C., and Wilson, D.A.-O. (2019). Odor Identification in Rats: Behavioral and Electrophysiological Evidence of Learned Olfactory-Auditory Associations. eNeuro *6*. https://doi.org/10.1523/ENEURO.0102-19.2019.

95. Huang, L., Ung, K., Garcia, I., Quast, K.B., Cordiner, K., Saggau, P., and Arenkiel, B.R. (2016). Task Learning Promotes Plasticity of Interneuron Connectivity Maps in the Olfactory Bulb. J. Neurosci. *36*, 8856–8871. https://doi.org/10.1523/JNEUROSCI.0794-16.2016.

96. Li, J., Luo, C., Peng, Y., Xie, Q., Gong, J., Dong, L., Lai, Y., Li, H., and Yao, D. (2014). Probabilistic diffusion tractography reveals improvement of structural network in musicians. PLoS One *9*, e105508. https://doi.org/10.1371/journal.pone.0105508.

97. Fuentes-García, J.P., Villafaina, S., Collado-Mateo, D., Cano-Plasencia, R., and Gusi, N. (2019). Chess Players Increase the Theta Power Spectrum When the Difficulty of the Opponent Increases: An EEG Study. Int. J. Environ. Res. Public Health *17*, 46. https://doi.org/10.3390/ijerph17010046.

98. Tamamaki, N., and Nojyo, Y. (1995). Preservation of topography in the connections between the subiculum, field CA1, and the entorhinal cortex in rats. J. Comp. Neurol. *353*, 379–390. https://doi.org/10.1002/cne.903530306.

99. Naber, P.A., Lopes da Silva, F.H., and Witter, M.P. (2001). Reciprocal connections between the entorhinal cortex and hippocampal fields CA1 and the subiculum are in register with the projections from CA1 to the subiculum. Hippocampus *11*, 99–104. https://doi.org/10.1002/hipo.1028.

100. Fyhn, M., Molden, S., Witter, M.P., Moser, E.I., and Moser, M.B. (2004). Spatial representation in the entorhinal cortex. Science *305*, 1258–1264. https://doi.org/10.1126/science.1099901.

101. Hargreaves, E.L., Rao, G., Lee, I., and Knierim, J.J. (2005). Major dissociation between medial and lateral entorhinal input to dorsal hippocampus. Science *308*, 1792–1794. https://doi.org/10.1126/science.1110449.

102. Ito, H.T., and Schuman, E.M. (2012). Functional division of hippocampal area CA1 via modulatory gating of entorhinal cortical inputs. Hippocampus *22*, 372–387. https://doi.org/10.1002/hipo.20909.

103. Li, X.G., Somogyi, P., Ylinen, A., and Buzsáki, G. (1994). The hippocampal CA3 network: an in vivo intracellular labeling study. J. Comp. Neurol. *339*, 181–208. https://doi.org/10.1002/cne.903390204.

104. Ishizuka, N., Cowan, W.M., and Amaral, D.G. (1995). A quantitative analysis of the dendritic organization of pyramidal cells in the rat hippocampus. J. Comp. Neurol. *362*, 17–45. https://doi.org/10.1002/cne.903620103.

105. Witter, M.P., Van Hoesen, G.W., and Amaral, D.G. (1989). Topographical organization of the entorhinal projection to the dentate gyrus of the monkey. J. Neurosci. *9*, 216–228.

106. Save, E., and Sargolini, F. (2017). Disentangling the Role of the MEC and LEC in the Processing of Spatial and Non-Spatial Information: Contribution of Lesion Studies. Front. Syst. Neurosci. *11*, 81. https://doi.org/10.3389/fnsys.2017.00081.

107. Igarashi, K.M., Ito, H.T., Moser, E.I., and Moser, M.B. (2014). Functional diversity along the transverse axis of hippocampal area CA1. FEBS Lett. *588*, 2470–2476. https://doi.org/10.1016/j.febslet.2014.06.004.

108. Deshmukh, S.S., and Knierim, J.J. (2011). Representation of non-spatial and spatial information in the lateral entorhinal cortex. Front. Behav. Neurosci. *5*, 69. https://doi.org/10.3389/fnbeh.2011.00069.

109. Ramírez-Amaya, V., Vazdarjanova, A., Mikhael, D., Rosi, S., Worley, P.F., and Barnes, C.A. (2005). Spatial exploration-induced Arc mRNA and protein expression: evidence for selective, network-specific reactivation. J. Neurosci. *25*, 1761–1768. https://doi.org/10.1523/JNEUROSCI.4342-04.2005.

110. Chawla, M.K., Guzowski, J.F., Ramirez-Amaya, V., Lipa, P., Hoffman, K.L., Marriott, L.K., Worley, P.F., McNaughton, B.L., and Barnes, C.A. (2005). Sparse, environmentally selective expression of Arc RNA in the upper blade of the rodent fascia dentata by brief spatial experience. Hippocampus *15*, 579–586. https://doi.org/10.1002/hipo.20091.

111. Soulé, J., Penke Z Fau - Kanhema, T., Kanhema T Fau - Alme, M.N., Alme Mn Fau - Laroche, S., Laroche S Fau - Bramham, C.R., and Bramham, C.R. (2008). Object-place recognition learning triggers rapid induction of plasticity-related immediate early genes and synaptic proteins in the rat dentate gyrus. Neural Plast. *2008*, 269097. https://doi.org/10.1155/2008/269097.

112. Satvat, E., Schmidt, B., Argraves, M., Marrone, D.F., and Markus, E.J. (2011). Changes in task demands alter the pattern of zif268 expression in the dentate gyrus. J. Neurosci. *31*, 7163–7167. https://doi.org/10.1523/JNEUROSCI.0094-11.2011.

113. Snyder, J.S., Ramchand, P., Rabbett, S., Radik, R., Wojtowicz, J.M., and Cameron, H.A. (2011). Septo-temporal gradients of neurogenesis and activity in 13-month-old rats. Neurobiol. Aging *32*, 1149–1156. https://doi.org/10.1016/j.neurobiolaging.2009.05.022.

114. Claiborne, B.J., Amaral, D.G., and Cowan, W.M. (1986). A light and electron microscopic analysis of the mossy fibers of the rat dentate gyrus. J. Comp. Neurol. *246*, 435–458. https://doi.org/10.1002/cne.902460403.

115. Kamondi, A., Acsády, L., Wang, X.J., and Buzsáki, G. (1998). Theta oscillations in somata and dendrites of hippocampal pyramidal cells in vivo: activity-dependent phase-precession of action potentials. Hippocampus *8*, 244–261. https://doi.org/10.1002/(SICI)1098-1063(1998)8:3<244::AID-HIPO7>3.0.CO;2-J.

116. Ormond, J., and McNaughton, B.L. (2015). Place field expansion after focal MEC inactivations is consistent with loss of Fourier components and path integrator gain reduction. Proc. Natl. Acad. Sci. USA *112*, 4116–4121. https://doi.org/10.1073/pnas.1421963112.

117. Schlesiger, M.I., Cannova, C.C., Boublil, B.L., Hales, J.B., Mankin, E.A., Brandon, M.P., Leutgeb, J.K., Leibold, C., and Leutgeb, S. (2015). The medial entorhinal cortex is necessary for temporal organization of hippocampal neuronal activity. Nat. Neurosci. *18*, 1123–1132. https://doi.org/10.1038/nn.4056.

118. Lopez-Madrona, V.J., and Canals, S. (2021). Functional Interactions between Entorhinal Cortical Pathways Modulate Theta Activity in the Hippocampus. Biology *10*, 692. https://doi.org/10.3390/biology10080692.

119. Grossberg, S. (2021). A Neural Model of Intrinsic and Extrinsic Hippocampal Theta Rhythms: Anatomy, Neurophysiology, and Function. Front. Syst. Neurosci. *15*, 665052. https://doi.org/10.3389/fnsys.2021.665052.

120. Jackson, J., Amilhon, B., Goutagny, R., Bott, J.B., Manseau, F., Kortleven, C., Bressler, S.L., and Williams, S. (2014). Reversal of theta rhythm flow through intact hippocampal circuits. Nat. Neurosci. *17*, 1362–1370. https://doi.org/10.1038/nn.3803.

121. Sandler, R.A., Song, D., Hampson, R.E., Deadwyler, S.A., Berger, T.W., and Marmarelis, V.Z. (2015). Model-based asessment of an in-vivo predictive relationship from CA1 to CA3 in the rodent hippocampus. J. Comput. Neurosci. *38*, 89–103. https://doi.org/10.1007/s10827-014-0530-8.

122. Makarov, V.A., Makarova, J., and Herreras, O. (2010). Disentanglement of local field potential sources by independent component analysis. J. Comput. Neurosci. *29*, 445–457. https://doi.org/10.1007/s10827-009-0206-y.

123. Lęski, S., Kublik, E., Swiejkowski, D.A., Wróbel, A., and Wójcik, D.K. (2010). Extracting functional components of neural dynamics with Independent Component Analysis and inverse Current Source Density. J. Comput. Neurosci. *29*, 459–473. https://doi.org/10.1007/s10827-009-0203-1.

124. Lasztóczi, B., and Klausberger, T. (2014). Layer-specific GABAergic control of distinct gamma oscillations in the CA1 hippocampus. Neuron *81*, 1126–1139. https://doi.org/10.1016/j.neuron.2014.01.021.

125. López-Madrona, V.J., Pérez-Montoyo, E., Álvarez-Salvado, E., Moratal, D., Herreras, O., Pereda, E., Mirasso, C.R., and Canals, S. (2020). Different theta frameworks coexist in the rat hippocampus and are coordinated during memory-guided and novelty tasks. eLife *9*. https://doi.org/10.7554/eLife.57313.

126. Robbe, D., and Buzsáki, G. (2009). Alteration of theta timescale dynamics of hippocampal place cells by a cannabinoid is associated with memory impairment. J. Neurosci. *29*, 12597–12605. https://doi.org/10.1523/JNEUROSCI.2407-09.2009.

127. Ito, H.T., Moser, E.I., and Moser, M.B. (2018). Supramammillary Nucleus Modulates Spike-Time Coordination in the Prefrontal-Thalamo-Hippocampal Circuit during Navigation. Neuron *99*, 576–587.e5. https://doi.org/10.1016/j.neuron.2018.07.021.

128. Ito, H.T., Zhang, S.J., Witter, M.P., Moser, E.I., and Moser, M.B. (2015). A prefrontal-thalamo-hippocampal circuit for goal-directed spatial navigation. Nature *522*, 50–55. https://doi.org/10.1038/nature14396.

129. Bourboulou, R., Marti, G., Michon, F.X., El Feghaly, E., Nouguier, M., Robbe, D., Koenig, J., and Epsztein, J. (2019). Dynamic control of

hippocampal spatial coding resolution by local visual cues. eLife *8*, e44487. https://doi.org/10.7554/eLife.44487.

130. Yu, J.Y., and Frank, L.M. (2021). Prefrontal cortical activity predicts the occurrence of nonlocal hippocampal representations during spatial navigation. PLoS Biol. *19*, e3001393. https://doi.org/10.1371/journal.pbio.3001393.

131. Oliva, A., Fernández-Ruiz, A., Buzsáki, G., and Berényi, A. (2016). Spatial coding and physiological properties of hippocampal neurons in the Cornu Ammonis subregions. Hippocampus *26*, 1593–1607. https://doi.org/10.1002/hipo.22659.

132. Rangel, L.M., Rueckemann, J.W., Riviere, P.D., Keefe, K.R., Porter, B.S., Heimbuch, I.S., Budlong, C.H., and Eichenbaum, H. (2016). Rhythmic coordination of hippocampal neurons during associative memory processing. eLife *5*, e09849. https://doi.org/10.7554/eLife.09849.

133. Sanders, H., Ji, D., Sasaki, T., Leutgeb, J.K., Wilson, M.A., and Lisman, J.E. (2019). Temporal coding and rate remapping: Representation of nonspatial information in the hippocampus. Hippocampus *29*, 111–127. https://doi.org/10.1002/hipo.23020.

134. Ku, S.P., Nakamura, N.H., Maingret, N., Mahnke, L., Yoshida, M., and Sauvage, M.M. (2017). Regional Specific Evidence for Memory-Load Dependent Activity in the Dorsal Subiculum and the Lateral Entorhinal Cortex. Front. Syst. Neurosci. *11*, 51. https://doi.org/10.3389/fnsys.2017.00051.

135. Mahnke, L., Atucha, E., Pina-Fernàndez, E., Kitsukawa, T., and Sauvage, M.M. (2021). Lesion of the hippocampus selectively enhances LEC's activity during recognition memory based on familiarity. Sci. Rep. *11*, 19085. https://doi.org/10.1038/s41598-021-98509-4.

136. Mathis, A., Mamidanna, P., Cury, K.M., Abe, T., Murthy, V.N., Mathis, M.W., and Bethge, M. (2018). DeepLabCut: markerless pose estimation of user-defined body parts with deep learning. Nat. Neurosci. *21*, 1281–1289. https://doi.org/10.1038/s41593-018-0209-y.

137. Ambard, M., and Rotter, S. (2012). Support vector machines for spike pattern classification with a leaky integrate-and-fire neuron. Front. Comput. Neurosci. *6*, 78. https://doi.org/10.3389/fncom.2012.00078.

STAR★METHODS

KEY RESOURCES TABLE

REAGENT or RESOURCE	SOURCE	IDENTIFIER
Chemicals, peptides, and recombinant proteins		
Ketamine	Bela-Pharm	Cat#N2703-15
NaCl 0.9%	Eifelfango	Cat#20029
Xylazine	WDT	00122
Atropine	Eifelfango	N/A
Meloxicam	Metacam	N/A
Lidocaine 0.5%	Carbostesin	N/A
Pentobarbital	Leibniz Institute for Neurobiology (Magdeburg, Germany)	N/A
Deposited data		
Source data	This manuscript	N/A
Experimental models: Organisms/strains		
Long-Evans rats	Janvier Labs	N/A
Software and algorithms		
LIBSVM	https://www.csie.ntu.edu.tw/~cjlin/libsvm/index.html	RRID:SCR_010243
DeepLabCut	https://doi.org/10.1038/s41593-018-0209-y	RRID:SCR_021391
Klustawik	http://klusta-team.github.io/klustakwik/	N/A
M-clust	https://redishlab.umn.edu/mclust	N/A
NanoZ (Multichannel systems)	https://www.multichannelsystems.com/software/nanoz	N/A
MATLAB R2022a	https://de.mathworks.com/products/new_products/release2022a.html	RRID:SCR_001622
Customized MATLAB codes	https://zenodo.org/records/11125633	N/A
Chronux toolbox	http://chronux.org/chronuxFiles/filesReleases/chronux_2_12.v03.zip	RRID:SCR_005547
Python 3.8	https://www.python.org/downloads/release/python-380/	RRID:SCR_008394
Customized python codes	https://zenodo.org/records/11125633	N/A
bycycle: cycle-*by*-*cycle* analysis of neural oscillations	https://github.com/bycycle-tools/bycycle.git	N/A
Other		
Stereotaxic frame	Kopf Instruments	N/A
Stereotaxic manipulator	Kopf Instruments	N/A
Tetrodes (tungsten wire, diameter 12μm)	California Fine Wire Company	N/A
Electrode microdrive	Axona	N/A
Recording systems	Axona; Neuralynx	N/A
Polylysine slides	Thermo Scientific	N/A
Video camera	Teledyne Dalsa	N/A
Cryostat CM 3050	Leica	N/A
Loop cereal	Kellogg's	N/A

RESOURCE AVAILABILITY

Lead contact

Further information and request for resources and materials should be directed to and will be fulfilled by the lead contact, Magdalena Sauvage (magdalena.sauvage@lin-magdeburg.de).

Materials availability

No unique materials have been generated in this study.

Data and code availability

- Data published in this manuscript are available upon request.
- All the original code has been deposited at Zenodo: https://zenodo.org/records/11125633. The DOI is listed in the key resources table.
- Any additional information required to reanalyze the data reported in this paper is available upon request.

EXPERIMENTAL MODEL AND STUDY PARTICIPANT DETAILS

Animals

Adult male Long–Evans rats [350–450 g; *n* = 10 in total] were maintained under reverse light/dark cycle (7:00 a.m. light off/7:00 p.m. light on) at a minimum of 90% of normal body weight, handled a week before the experiment, and tested in their home cage. All procedures were approved by the animal care committee of the State of Saxony-Anhalt (42502-2-1555 LIN) and performed in compliance with the guidelines of the European Community and ARRIVE guidelines.

METHOD DETAILS

Surgery

Once animals learned the task (see 'Behavioral paradigm and training' section) an electrode microdrive housing 16 individually movable tetrodes was implanted (Axona Ltd, St. Albans, UK, http://www.axona.com/). Tetrodes were arranged in 3 rows targeting the right dorsal hippocampus and covering the whole proximodistal axis of CA1 and CA3 from AP -3.,3 to AP -4 mm. Tetrodes, made of four tungsten wires (12 μm diameter each, California Fine Wire Company, Grover Beach, CA), were twisted and heated to form a bundle. The tips of tetrodes were cut and gold-plated (Sifcoasc, OH, USA, Gold NC SPS 5355) to reach an impedance <150kΩ with a NanoZ (Multichannel system, Reutlingen, BW, Germany). Animals were anesthetized by induction with 3% isoflurane and injected with Ketamin/Xylavet (75 mg/kg and 5 mg/kg) mixture and Atropine (0.1 mg/kg) to facilitate breathing. Once deeply anesthetized, animals were placed in the stereotactic frame (David Kopf Instrument, CA, USA) fitted with a gas mask supplying 1% isoflurane and 0.8–1.2L/min oxygen. Local anesthesia (Lidocaine, 0.5%, < 7 mg/kg) was injected subcutaneously before incision. Analgesic agent Metacam (5 mg/kg) was injected 2 h after the injection of the Ketamine cocktail. A craniotomy was performed above the targeted hippocampal area (AP -2.5∼-4.5, ML 1.2–4.2, right hemisphere). Six anchoring stainless screws (1mm diameter, 3-4mm long) were placed into the skull above the prefrontal, left hemisphere and cerebellar areas. A silver wire was twisted around the two cerebellar screws to serve as grounding (reference) electrodes and soldered onto the contact point of the microdrive at a later time. Note that the distance between distal CA1 tetrodes and the ground screws is comparable to that of proximal CA1 tetrodes to ground screws. After removing the dura using a dura hook (Fine Science Tools, Heidelberg, Germany) tetrodes were lowered to 800∼1000μm below cortex surface. A mixture of melted paraffin wax/oil (wax:oil 3.5:1, Aldrich) was dropped along the tetrodes (covering the craniotomy), and the drive was secured with dental cement (Paladur, Heraeus, Hanau, Germany). Animals were supplied with oral analgesic meloxicam (0.5 mg/ml, 2.6 mL/kg) once a day for 3 days and recovered for a duration of one week. Tetrodes were then slowly lowered to the regions of interest into the pyramidal layers of CA1 and CA3 over 2 weeks.

Behavioral stimuli

The stimulus odors were common household scents (thyme, paprika, coriander, etc.) mixed with playground sand. The scented sand was held in glass cups (one odor per cup), and a cup was fixed on a small platform lowered in the front part of the cage for testing. A pool of 40 household odors was available, 20 were used each day chosen in a pseudo random manner.

Behavioral paradigm and training

To test the non-spatial recognition memory, we used the innate ability of rats to dig and to discriminate between odors. Behavioral training and paradigm have been described in details previously.[51,134,135] In short, each training session contained a "study" phase, a delay, and a "test" phase. Each day, rats were presented with a study list of 10 odors, which was different each day. Odors were chosen in a pseudo random manner. During the recognition, i.e., the "test" phase, animals were tested for their ability to distinguish between the 10 odors presented during the study phase ("repeated" odors) and 10 additional odors ("non-repeated" odors) that were part of the pool of forty odors, but were not presented during the study phase. To do so, rats were first trained to dig in the stimulus cups with unscented sand to retrieve one 1/4 of piece of loop cereal (Kellogg's) after which animals were trained on a delayed non-matching to sample rule. During the "test" phase, when rats were presented with an odor that was part of the study list (a "repeated" odor), rats were required to refrain digging, turn around, and go to the back of the cage to receive a food reward: a correct response for a "repeated" odor (Figure 1B; an incorrect response would be digging in the stimulus cup). Conversely, when the odor was not part of the study list (a "non-repeated" odor), animals could retrieve a buried reward by digging in the test cup: a correct response for a "non-repeated" odor (an incorrect response would be going to the back of the cage to receive the reward). To ensure

that the task could not be solved by smelling the reward buried in the sand, crushed cereals were mixed in the sand of all stimulus cups. In addition, no spatial information useful to solve the task was available to the rats, given that testing cups for 'repeated' and 'non-repeated' 'odors were presented at the exact same location. Reward locations differed for the 'non-repeated' and the 'repeated' odors (front and back of the cage, respectively), but were only experienced by the animals once a decision had been made (e.g., when the trial was over), hence could not contribute to behavioral performance. Training lasted for about 2 months and consisted of several steps, during which the number of studied odors increased from 1 to 10, the delay increased from 1 to 20 min, and the number of odors during the test phase increased from 2 to 20 (10 'repeated' and 10 'non-repeated' intermixed). Animals transitioned between successive training stages when performance reached a minimum of 75% correct for 3 consecutive days. Once this criterion was reached for the final training stage (10 study odors, 20 min delay, and 20 test odors), animals were further trained for at least another week and implanted with a microdrive. Following one week of recovery period, neurons were screened and animals trained back to criteria following which they were recorded for one additional session that was used for the analyses. Memory performance on the recording day was 80% on average (Table S1A).

Animal's local motion was minimized by using a 35 × 19 cm cage. The behavior of the animals was recorded and streamed to a computer with a high-speed, HD infrared camera (100 fps, Genie Nano Series, GigE Vision, Teledyne Dalsa, Ontario, Canada). The camera sent one trigger per frame to the recording system to synchronize video and electrophysiological recordings. Behavioral performance was assessed with high temporal resolution (10 ms precision). Periods analyzed started upon stimulus presentation (when the front edge of the platform on which the stimulus cup was fixed crossed the wall of the cage, Figure S1) and ended 2 s later: i.e., for the 'test' phase: before the turning or digging behavioral responses. The time-window of 2 s was defined based on prior experiments showing that behavioral responses in this task occurred shortly after 2 s. Rats were sniffing and alertly waiting during these periods.

For trained rats, free-run was performed in an 80 × 80 × 10cm square arena (open top, customized) following the delayed non-matching to odor task, after animals rested for 20 min in their home-cage. The arena was placed in the recording booth and animals could foraged for cereals (cheerios) scattered on the floor. A freerun session lasted 8 min. Behavioral and electrophysiological signals were recorded with the camera and recording systems used while animals performed the task. The same freerun procedure applied to naive controls, except that animals did not undergo the two-month training on the task, but were housed in the same facility and brought to the experimental room as frequently as experimental animals. Naive animals were implanted with the same recording drive (16 tetrodes) as trained animals and recorded after one week of recovery as was the case for trained animals. The recording session for naive rats lasted about 30 min and consisted of 20 min resting time (home cage) and 8 min freerun.

Histology and reconstruction of recording positions

After the final recording, animals were overdosed with pentobarbital (500 mg/ml, IP) before intracardiac perfusion with 0.9% saline and 4% formaldehyde. The brain was extracted and post-fixed with 4% formaldehyde for 24 h. Brains were then transferred to a 30% sucrose solution for cryoprotection and subsequently frozen at −41°C in isopentane using dry ice and stored in −80°C. Brains were cut into 30 μm coronal sections with a cryostat (Leica CM3050S, Leica Microsystems), mounted on glass slides and stained with cresyl violet (Nissl staining). The tips of the tetrodes were identified from the stained brain slices.

Data acquisition

The electrophysiological signals were recorded with an Axona system (Axona Ltd, St. Albans, UK) in one animal (LE46) and with a Neuralynx (Neuralynx, Bozeman, MT, USA) data acquisition system in the rest of animals (4 trained, 5 naive). With the Axona system, the signals were preamplified with headstages (Axona, 2 × 32 channels) and digitized at 24 kHz. In addition to this broad band raw signal, the Axona system created down-sampled data for LFP analysis by low pass-filtering the broad band signal at 2400 Hz, and down-sampling it to 4800 Hz. With the Neuralynx system, signals were preamplified with headstages (Neuralynx, 2x32 channels), digitized at 32 kHz then the broad band signals were recorded.

QUANTIFICATION AND STATISTICAL ANALYSIS

Behavior

Memory performance

The performance of animals (% correct choice) were calculated by evaluating the number of correct trials during the test period divided by all testing trials (20) and multiplying by 100.

Speed analysis

To ensure that theta amplitude differences between task periods do not solely stem from animals' motion, the speed of the animals was assessed using DeepLabCut software package.[136] Because of the similarity in behavior across animals (n = 5), 'study' and 'test' video clips were pooled together to train one network. For the same reason, baseline video clips of trained (n = 5) and naive (n = 5) animals were also pooled together. Freerun videos were pooled to train a third independent network. 50 frames per video were randomly extracted, and the nose, ears and 3 points along the midline of the body (neck, mid of the body and tail base) were manually labeled on each frame. The networks were trained with default parameters and 200 000 iterations. The trained networks and frames were then manually evaluated to analyze the entire videos.

Given that the body of the animals was virtually immobile during the present task, the position of the mid-point of the two ears was used to estimate the speed of the animals in an attempt to prevent an under estimation of the speed of movements. The instantaneous moving speed was estimated based on the displacement of the labels occurring between two consecutive frames, to which a Kalman filter was applied.[100] The speed of individual animals was calculated by pooling the 2 s trials together and the median of the speed distribution was used to represent the speed because of the nonnormal distribution of the speed across the task phases. For baseline and freerun periods, 20 periods of 2 s each were randomly selected and the same procedure applied.

Spike sorting

The broadband data (sampled at 24 kHz or 32 kHz) were filtered between 500 and 8000 Hz and an automatic clustering procedure applied using klustakwik (http://klusta-team.github.io/klustakwik/). The parameters were as follows: action potentials with power of >4 standard deviations from the baseline mean were selected and their spike features were extracted with principal component (PC) analysis. Using the first 3 PCs and the initial cluster was set to 100. Afterward the clusters were manually selected, combined or split with the software klusters (http://klusta-team.github.io/klustakwik/) or M-clust (https://redishlab.umn.edu/mclust), selecting only the clusters with clear refractory periods in their autocorrelation, well-defined boundaries and stability over time.

Support vector machine (SVM)

The performances for classifying the two testing trial types ('repeated' or 'non-repeated' odors during test period) with either the population spiking activities or the theta phases of population CA3 or CA1 spikes were assessed with the support vector machine method[58,137] using software LIBSVM (https://www.csie.ntu.edu.tw/∼cjlin/libsvm/index.html). A polynomial kernel was used with default parameters.

The leave-1-out cross validation procedure was used to evaluate the accuracy of SVM classification performances. In brief, for each iteration, the population neuronal activities of one trial was left out of the dataset and the data of the rest of the trials (19 out of 20) were used to train the SVM. The trained SVM was then tested with the trial left out in the current iteration. The same procedure was performed for each trial without repetition. Finally, The SVM performance was calculated by counting how many iterations yielded a correct output. Since the test phase of the task consists of 10 'repeated' and 10 'non-repeated' trials, chance level mount to 50% correct. Given the total number of test trials, a minimum reduction in performance is 5% (1/20 trials).

For population spiking activities, the combined mean firing rates of the 2 s following stimulus presentation during retrieval phase of each neuron were used as 'features.' To test whether the hippocampal population firing predicted the type of stimulus presented ('repeated' vs. 'non-repeated') or behavioral responses ('digging' or 'turning' independently of whether animals were correct or not), the SVM were trained separately with the labels 'stimulus types' or 'behavioral responses.' For population theta phases, the circular mean of the theta phases of each 2-s trial was calculated for each neuron and the circular means of the theta phases of all neurons per trial used to perform the SVM-training and the cross validation. Of note, for theta phase analyses, only the neurons which spiked for each of the 20 test trials were used. Neurons which did not fire at each trial were excluded since the mean theta phase could not be calculated for all trials.

Selection of 'effective' neurons

To find out which neuron contributed ''effectively'' to the SVM performance, i.e., which neurons would cause a significant decrease of SVM performance if removed, an iterative feature selection procedure was applied to the neurons of each animal (Figure S3). For each iteration, each neuron was deleted one at a time from the pool of recorded neurons ($n = N$). The effectiveness score (ES) was calculated by subtracting the performance of all recorded neurons (perf all, $n = N$) from the performance of the remaining neurons (perf (N-1), $n = N$-1) to assess if the deletion of one specific neuron affected the population classification performance. If that was the case (ES < threshold), the neuron was termed 'effective' neuron, if not: 'non-effective' neuron. Once tested, each deleted neuron was placed back to the pool of neurons, and the next iteration started with the deletion of the next neuron (without repeating sampling). The procedure was illustrated in Figure S3.

To evaluate the ES threshold, the features of the 20 trials were bootstrapped 1000 times and a 5%-decrease in SVM performance was found to be significant with 95% confidence interval, hence set as a (ES) threshold. To further ensure that removing one effective neuron caused a significant reduction in SVM performance, the dataset of the target/studied neuron was replaced by randomly selecting 20 data points from the remaining N-1 neurons (i.e., out of 20 X (N-1) data points), the SVM analysis was performed with this new dataset (in total N neurons) and this procedure repeated 1000 times. Doing so, we found that the SVM performance of this new dataset ($n = N$) was comparable to the performance of the N-1 dataset (i.e., 5% lower than the performance of all neurons) despite the same sample size ($n = N$), indicating that the drop in performance did not stem from the sample size alone and that removing the 'effective' neuron significantly affects the SVM performance.

To evaluate whether the distribution of 'effective' neurons is homogeneous along the proximodistal axis of CA1 or CA3 and compare across animals, the recording sites of 'effective' and 'non-effective' neurons was sorted into 5 CA1 and CA3 segments for each animal and the count of neurons were summed across animals for each segment (Figure 2D; Table S2). The proportion of 'effective' neurons was calculated by dividing the sum of 'effective' neurons by the total number of neurons recorded (effective + non-effective across animals) for each segment and a linear regression model with a least square approach was fitted to the CA1 and CA3 data.

Analyses

The local field potential (LFP) recorded with the Axona system (4800Hz) were directly used for further analysis; the broadband signals recorded with the Neuralynx system (32 kHz) were low-pass filtered with a cutoff frequency 300 Hz using MATLAB filter function and then down-sampled 8 times to 4 kHz. Toolbox Chronux (version 2.12 v03) was used to obtain the theta power and to estimate the theta phases using multi-taper method (taper = 5–9). The cycle-by-cycle theta amplitudes were obtained with the toolbox bycycle (https://github.com/bycycle-tools/bycycle,[60]). Theta frequency was defined as oscillations between 6 and 12 Hz.

For each animal, theta cycle amplitudes of all trials (10–20 cycles/trial) in a specific task phase were pooled together (see Figures 3C, 3D, and 4 for distributions in a representative animal), subsequently to which a group analysis on trained ($N = 5$) and naive animals ($N = 5$) was performed. Population differences in theta amplitudes were calculated using the Kolmogorov–Smirnov (KS) test to generate D values (D = Maximum|Fo(X)−Fr(X)|, X = theta cycle amplitudes, F(X) = observed cumulative frequency distribution of a random sample of n observations) and Friedman's test was performed on these values to obtain group statistics.

For testing whether neuronal firings were phase-locked to theta oscillations, circular Rayleigh test was used. To test whether the theta phases of neuronal spiking can discriminate different stimulus types ('repeated' vs. 'non-repeated' odor), theta phases of one specific neuron were pooled together for 'repeated' or 'non-repeated' trials and compared with the circular Watson-Williams multi-sample test for equal variance (threshold $p < 0.05$, MATLAB Circular Statistic toolbox, Philipp Berens 2023, https://www.mathworks.com/matlabcentral/fileexchange/10676-circular-statistics-toolbox-directional-statistics). When the difference in theta phases between 'repeated' and 'non-repeated' trials surpassed the threshold ($p = 0.05$, two-tailed), the neuron was termed 'phase-discriminating;' when it did not, the neuron was termed 'non-phase discriminating.. The phase-discriminating neurons were subdivided into two categories: type I neurons, phase-locked to the same angle of CA1 theta oscillations for both 'repeated' and 'non-repeated' odors and type II neurons, phase-locked to only one stimulus type. Of note, due to the very low error rate (memory performance on recording day was 80% on average i.e., 16 correct trials out of 20; for each condition 8 out of 10 correct trials) only 2 error trials per animal on average were available for analyses. All the trials (correct or incorrect) were used in the analyses.

In order to test how local spike-theta phase-locking in CA3 or CA1 may contribute to the test phase of the non-spatial memorytask, we obtained the theta phases of the CA3 or CA1 spikes using the theta oscillations recorded with the same tetrode as reference. Then the phases referenced to local theta oscillations were compared to the phases using the distal CA1 theta as reference to compare which phase-information can predict behavior performance better to assess whether local or cross-area theta phase locking may play an important role during the test phase of the memory task. The procedure was as follows: for each animal the different theta phase information (CA1 spike - local CA1 theta phase, CA3 spike - local CA3 theta phase and CA3 spike-distal CA1 theta phase) was used to perform SVM analysis according to the description in "Support Vector Machine (SVM)" section. Subsequently, one-way ANOVA was applied to the SVM performances predicted by the three spike-theta conditions (CA1 spikes -CA1 theta, CA3 spikes -CA3 theta and CA3 spikes-distCA1 theta) to directly compare the performances of each condition. Then a post-hoc analysis was performed to test whether the CA3 spike-distCA1 theta phase information did outperform the local theta phase information.

Generalized linear mixed effect (GLME) model

We asked whether theta-amplitudes depend on memory task-phases and/or running speed in the present study by performing the GLME model, using the task phases, running speed and their interaction as fixed effects and animals as a random effect. MATLAB's fitlme function (with default parameters) was used for performing GLME analysis.

Statistical analysis

Analyses were performed using custom written MATLAB (R2020a) or python scripts (version 3.8). The normality of all distributions were tested with Lilliefors test. When data were normally distributed, ANOVA and one-or two-tailed t-tests were used. For chance level or two-group comparisons in non-normally distributed datasets, the Mann-Whitney U test was used. Of note, paired two-group comparisons could not be performed due to unequal number of observations in different groups. The Friedman's test was used for comparisons of more than two groups in non-normally distributed datasets. For proportion comparisons, two-sample z-test

was used. For testing dependencies of two variables, linear regression analysis was used. To compare directly the phase-locking of CA3 spikes to distal and proximal CA1 theta for repeated and non-repeated stimuli, we calculated the circular distances of each neuron's mean phase to the circular median ([66] p. 637) of each condition and further performed a circular HKtest,[67] a two-way ANOVA corresponding test for circular data, to compare the phase dispersions of each condition. The significance threshold of all tests with multiple comparisons were false discovery rate (FDR) corrected. Statistical tests used and p values are reported in the text, tables or figure legends. ($^*p < 0.05$, $^{**}p < 0.01$, $^{***}p < 0.001$). Error bars indicate the S.E.M.